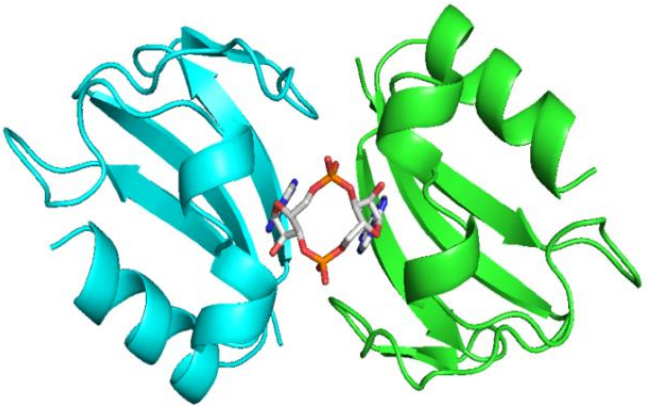

Biochemical Characterization of KhtTU, a K^+/H^+ Antiporter from *Bacillus subtilis*

João Pedro Leitão Guerra

Mestrado em Bioquímica

Departamento de Química e Bioquímica

2017

Orientador:

João Morais Cabral, Investigador Principal, IBMC - i3s

Todas as correções determinadas pelo júri, e só essas, foram efetuadas.
O Presidente do Júri,

Porto, _____/_____/_____

Agradecimentos

Gostaria de expressar o mais profundo agradecimento:

A João Morais Cabral, pela oportunidade de realizar este projecto e por toda a confiança, orientação e influência no meu desenvolvimento pessoal e profissional;

A Carol Harley, por todo o apoio, paciência e acima de tudo por todos os ensinamentos e conselhos ao longo deste ano;

Ao Celso Duarte, pelo companheirismo, assistência, motivação e partilha de conhecimentos e amizade;

Aos restantes membros do grupo: Andreia, Rita, Artur, João Jorge e Patrícia, pelo fantástico ambiente de equipa, amizade e apoio;

A todos os meus amigos, em especial ao Vasco Fontes, Ana Spencer, Daniel Botto, Pedro Rodrigues, Ricardo Martins e Pedro Baptista, Padrinhos e Afilhados, responsáveis pelos momentos mais inesquecíveis, por estarem presentes todos os dias, perto ou longe;

Ao Diogo Gomes, pela maior das amizades, desde sempre;

À minha Mãe, Pai, Irmão e Avós, por todo o amor e carinho, por tudo aquilo que sou e alcancei.

À Ana, por tudo.

Resumo

O potássio (K^+) é o catião intracelular mais abundante em todos os domínios da Vida. De modo a garantir a concentração apropriada deste elemento, todos os organismos tiveram que desenvolver sistemas proteicos responsáveis pela homeostasia de K^+. No organismo modelo de bactérias Gram-positivas *Bacillus subtilis* estão presentes diversos transportadores de potássio. Um destes é o antiportador de K^+/H^+ KhtTU, um transportador envolvido na regulação do pH e da pressão osmótica deste organismo. Este antiportador é composto pela proteína transmembranar KhtU, responsável pelo fluxo de iões e pela proteína citosólica reguladora KhtT. A principal intenção deste projecto foi a de caracterizar as propriedades moleculares deste antiportador.

Durante o curso deste trabalho foram estabelecidos os protocolos de expressão e purificação em larga-escala da proteína KhtT e do complexo KhtTU. O mensageiro secundário di-AMP cíclico (c-di-AMP), essencial para alguns processos celulares deste organismo incluindo a homeostasia de potássio, foi identificado como ligando da KhtT. A caracterização das propriedades moleculares desta interação demonstrou que a mesma acontece com alta afinidade e especificidade e estabiliza a estrutura da proteína. Ensaios de calorimetria de titulação isotérmica (ITC) definiram o valor de 138 nM como a constante de dissociação desta ligação. Ensaios funcionais usando vesículas invertidas contendo o complexo KhtTU revelaram que o c-di-AMP actua como activador do antiporte, aumentando a sua constante de velocidade de fluxo quase 10 vezes. Com este ensaio foi estimado o valor de 1.97 μM para o EC_{50} de activação. Foram ainda feitos ensaios cristalográficos na tentativa de obter a estrutura da KhtT com c-di-AMP associado, que resultaram na determinação e optimização de uma condição. Vários conjuntos de dados com resolução até 2.3 Å foram recolhidos mas a determinação da estrutura da proteína não foi concluída.

Palavras-chave: Homeostasia de potássio, antiportador, proteína de membrana, KhtTU, KhtT, KhtU, di-AMP cíclico, domínios RCK, cristalografia.

Abstract

Potassium (K^+) is the most abundant intracellular cation in all cells. In order to ensure proper intracellular levels of this element all organisms evolved a potassium homeostasis system. *Bacillus subtilis*, a Gram-positive bacterium, possesses several potassium transporters. The KhtTU protein complex is a *B. subtilis* K^+/H^+ antiporter, a still largely uncharacterized protein with established roles in alkali resistance and osmoregulation. This antiporter is composed by the membrane protein KhtU, responsible for ion flux, and the cytosolic regulatory protein KhtT. The major aim of this project was to characterize the molecular properties of this antiporter.

This work established large-scale expression and purification protocols for KhtT and KhtU (as a KhtTU complex). Cyclic di-AMP (c-di-AMP), an important second messenger in Gram-positive bacteria and potassium homeostasis, was identified as a ligand of KhtT. Biochemical characterization of this interaction showed that binding occurs with high affinity (dissociation constant of 138 nM determined by ITC), specificity (cyclic di-GMP does not bind) and induces a structural stabilization of the protein. Functional assays of KhtTU in everted vesicles revealed that c-di-AMP acts as an activator of antiporter activity, enhancing transport rate almost 10-fold. Using this assay it was determined that the EC_{50} of activation for c-di-AMP is 1.97 μM. Crystallization trials for KhtT in the presence of c-di-AMP were carried out and one workable condition was optimized. Several datasets with resolution as high as 2.3 Å were collected. However, the determination of the protein structure was not concluded.

Keywords: Potassium homeostasis, antiporter, membrane protein, KhtTU, KhtT, KhtU, cyclic di-AMP, RCK domain, crystallography.

Table of Contents

List of Tables

Appendix:

List of Figures

Appendix:

List of Abbreviations

Å	Ångström
A_{280nm}	Absorbance at a wavelength of 280 nanometers
aa	Aminoacids
ACMA	9-Amino-6-Chloro-2-Methoxyacridine
ADP	Adenosine diphosphate
ATP	Adenosine triphosphate
BSA	Bovine Serum Albumin
BSH	Bacillithiol (reduced)
Ca^{2+}	Calcium ion
c-di-AMP	Cyclic di-adenosine monophosphate
c-di-GMP	Cyclic di-guanosine monophosphate
cm	Centimeter
CPA	Cation-Proton Antiporter family
CPA2	Cation-Proton Antiporter 2 subfamily
CVs	Column Volumes
cytS	84-aminoacids long segment between amino acids 29 and 112 of KhtS
Da	Dalton
DDM	n-Dodecyl-β-D-maltopyranoside
DNA	Deoxyribonucleic acid
DSF	Differential Scanning Fluorimetry
DTT	Dithiothreitol
E-BSH	Ethylmaleimide-Bacillithiol (oxidized form of BSH)
ECL	Enhanced chemoluminescence
EC_{50}	Half maximal effective concentration
H^+	Hydrogen ion / Proton
HCl	Hydrochloric acid
HEPES	4-(2-hydroxyethyl)-1-piperazineethanesulfonicacid
His/His_6	Hexahistidine tag
IMAC	Immobilized Metal Affinity Chromatography
IPTG	Isopropyl β-D-1-thiogalactopyranoside
ITC	Isothermal Titration Calorimetry
k / k_{fast} / k_{slow}	Rate constants
K^+	Potassium ion
K_2HPO_4	Potassium phosphate dibasic
K_A	Association constant

kcal	Kilocalories
KCl	Potassium Chloride
K_D	Dissociation constant
KH_2PO_4	Potassium phosphate monobasic
LB	Lysogeny broth
LBK	Lysogeny broth with potassium
Li^+	Lithium ion
M	Molar
MCS	Multiple Cloning Site
mg	Miligram
$MgCl_2$	Magnesium Chloride
mL	Mililiter
mM	Milimolar
Na^+	Sodium ion
NaCl	Sodium Chloride
NAD^+	Nicotinamide adenine dinucleotide, oxidized
NADH	Nicotinamide adenine dinucleotide, reduced
NaOH	Sodium hydroxide
NH_4^+	Ammonium ion
Ni^{2+}	Nickel ion
NiNTA	Nickel-nitrilotriacetic acid
nm	Nanometer
OD	Optical density
ON	Overnight
ORF	Open Reading Frame
PCR	Polymerase Chain Reaction
PDB	Protein Data Bank
PEG	Polyethylene Glycol
PMSF	Phenylmethane sulfonyl fluoride
psi	Pounds per square inch
Rb^+	Rubidium ion
RbCl	Rubidium Chloride
RCK	Regulator of conductance of K^+
RCK_C	C-terminal subdomain of an RCK domain
RCK_N	N-terminal subdomain of an RCK domain
RFU	Relative fluorescence units

RNA	Ribonucleic acid
rpm	Revolutions per minute
SD	Standard Deviation
SDS	Sodium dodecyl sulfate
SDS-PAGE	Sodium dodecyl sulfate polyacrylamide gel electrophoresis
SEC	Size-exclusion chromatography
SeMet	Selenomethionine variant
SL-BSH	S-lactoyl-bacillithiol
T	Temperature
TB	Terrific Broth
TBS	Tris-buffered saline
TCEP	Tris(2-carboxyethyl)phosphine
TFA	Trifluoroacetic acid
Thr	Thrombin
Tm (ºC)	Melting Temperature
Tris	Tris(hydroxymethyl)aminomethane
tRNA	Transfer RNA
TSA	Thermal Shift Assay
α	Anti
Δ	Variation
ε	Molar extinction coefficient
λ	Wavelength
µcal	Microcalories
µg	Microgram
µL	Microliter
µM	Micromolar
µM	Micromolar

1. Introduction

1.1. Potassium in Biology

The ionic content of the cytosol is usually much different from that of the extracellular fluid. In essentially all cells cytosolic pH is maintained close to 7.2 and the concentration of potassium (K^+) is much higher than sodium (Na^+) [1]. In fact, K^+ is the most abundant intracellular cation in both bacteria and eukaryotes [2]. All living cells accumulate K^+ to achieve internal concentrations of this cation higher than and relatively independent of those outside [3]. In *Escherichia coli*, for example, K^+ is accumulated up to 400 mM [4]. In *Bacillus subtilis,* a potassium pool of about 350-600 mM has been reported [5,6]. In human cells, its levels are kept around 140 mM, while other cations such as sodium (Na^+) and calcium (Ca^{2+}) have much lower intracellular concentrations (12 mM and <0.2 µM, respectively)[1].

Potassium serves multiple purposes: besides acting as a compatible solute to counteract osmotic stress[7–9] and being required for maintaining intracellular pH [10,11], it also affects gene expression[12], biofilm formation[13], activation of intracellular enzymes[14] and is necessary for ribosome function [15,16]. In more advanced organisms, such as mammals, potassium is also used to generate a membrane potential, critical for highly important processes such as neurotransmission[17,18], muscle contraction [19,20] and heart function [21,22].

One of the factors that determine K^+ levels in bacteria is cell turgor pressure. A significant increase in medium osmolarity stimulates K^+ influx. This increase in the potassium pool serves as the first line of defense against loss of water and leads to a regain of turgor [9]. Conversely, when cells adapt to media of lower osmolarity, the increase in turgor stimulates K^+ efflux [3]. Changes in cellular K^+ concentration alter turgor while turgor is implicated as a signal-controlling activity of K^+ transport systems [2].

In order to ensure the appropriate intracellular levels of potassium all organisms had to evolve potassium homeostasis systems, regulating both its influx and efflux.

1.2. Potassium Homeostasis in *Bacillus subtilis*

Since the external concentration of potassium is usually low (only 100 μM to 10 mM in typical bacterial habitats), efficient uptake and intracellular enrichment of the ion is necessary. Most bacteria possess multiple potassium uptake systems to allow efficient transport under different environmental conditions [4].

Many of the prokaryotic ligand-gated K^+ channels and some eukaryotic channels are composed of two components: a functional domain consisting of a transmembrane tetrameric pore through which ions flow and a regulatory component consisting of cytosolic ligand-binding domains called "regulator of K^+ conductance" (RCK) domains [23], in an assembly similar to the examples shown in **Figure 1.1**.

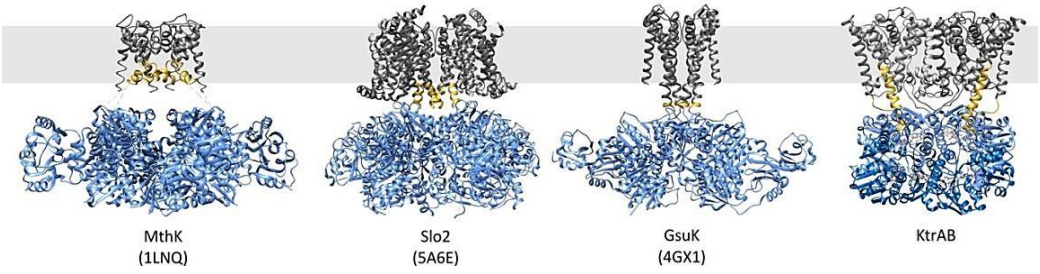

Figure 1.1 - Schematic representation of the general assembly of a potassium channel. It is usually composed of two parts: a transmembrane component containing the pore through which potassium ions pass and an oligomeric peripheral regulator component usually containing an RCK domain (regulator of conductance of K^+). Legend: Side views of MthK (PDB code: 1LNQ), Slo2 (PDB code: 5A6E), GsuK (PDB code: 4GX1) and ADP-bound KtrAB. Membrane domains in grey; flexible linker or extended helices in yellow; octameric RCK domains in blue. The grey bar represents the membrane. Adapted from [24].

The basic assembly unit of these regulatory domains is a homodimer of RCK subunits. Each one of these domains can be subdivided into two subdomains: the N-terminal subdomain (termed RCK_N) and the C-terminal subdomain (RCK_C), usually connected by a linker region [25], as shown in **Figure 1.2**. Four of these homodimer units then assemble as an octamer, acquiring the architecture shown above.

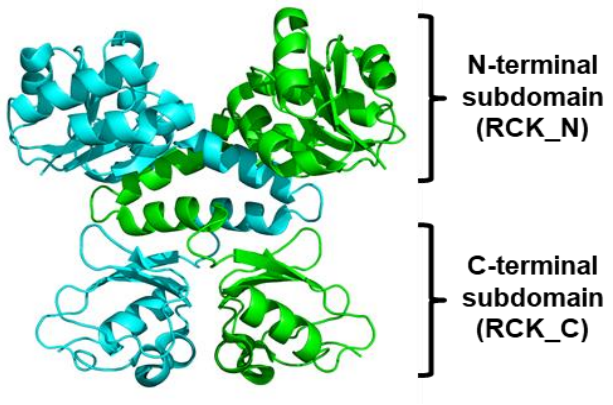

Figure 1.2 - Representation of the RCK homodimer unit of a prokaryotic potassium channel.
Depiction of the homodimer unit of the RCK domain of MthK, a K^+ channel from *Methanothermobacter thermoautotrophicus* (PDB code: 1LNQ). Four of these homodimers bind to each other, assembling the regulatory component of the channel, in the form of an octamer. Each monomer is colored in either cyan or green.

Different ligands have been identified for RCK domains present in the potassium transport machinery of different organisms, such as ATP/ADP[26], NADH/NAD^+ [27] or divalent cations such as Ca^{2+} [28]. A general mechanism has been proposed for the way RCK domains regulate the activity of the channels [24]. In brief, the binding of a ligand to these domains leads to a conformational change that is propagated to its transmembrane counterpart, leading to a more open state of the channel, increasing the flow of K^+ [23,24].

In the Gram-positive model organism *Bacillus subtilis* three different potassium importers have been found: KtrAB and KtrCD [8], which consist of a transmembrane channel-like subunit (KtrB or KtrD) and a peripheral regulatory subunit (KtrA or KtrC); and KimA [29]. The KtrA and KtrC regulatory subunits of the KtrAB and KtrCD transporters are RCK domains and exhibit the ability to control the activity of the transporter subunit by binding nucleotides [25]. Crystal structures of KtrAB have been obtained (PDB code: 4J7C) [26,30], revealing a complex architecture of a dimer of KtrB bound to a cytosolic octameric ring formed by homodimeric KtrA units (see **Figure 1.1**, to the right).

Thus, *Bacillus subtilis* is equipped to acquire potassium from the extracellular media. However, prolonged high levels of potassium ions are detrimental to cellular physiology, mostly when turgor is dangerously high. At this point, potassium efflux is required [9]. The only well-characterized K^+ efflux systems in bacteria are the *E. coli* glutathione-gated KefB and KefC systems.[31,32] These are potassium-proton (K^+/H^+) antiporters composed of transmembrane subunits (KefC or KefB) bound to cytoplasmic ancillary subunits (KefF or KefG) [33]. In contrast, potassium extrusion in *B. subtilis* is not completely understood, with two putative K^+ export pathways proposed: the YugO channel[13,34] and the cation-proton antiporter KhtTU [35].

1.3. The *khtSTU* Operon

The cation/proton antiporters (CPAs) superfamily of proteins is generally divided into 4 subfamilies. One of which is the CPA2 subfamily. This family of antiporters includes proteins present in different bacteria, archaea and eukaryotes such as the aforementioned *E. coli* K^+/H^+ antiporters KefFC and KefGB, the *Enterococcus hirae* Na^+/H^+ antiporter NapA or the *Bacillus pseudofirmus OF4* $NH_4^+(K^+)/H^+$ antiporter AmhMT. [35] These antiporters have roles in resistance to diverse cytotoxic cations, alkali resistance, electrophile resistance and osmoregulation.

The *khtSTU* operon of *Bacillus subtilis* encodes potassium-transport-related proteins that exhibit sequence similarity to CPA2 family members. [36] According to two reference genome databases for *Bacillus subtilis*, *SubtiList* [37] and *SubtiWiki* [38], this operon consists of 3 different ORFs: *khtU*, *khtT* and *khtS* (**Figure 1.3**). The *khtU* gene encodes a transmembrane protein with high sequence similarity to the cation/proton antiporter family, with a theoretical size of 44 kDa and 408 amino acids per subunit. Located upstream of *khtU*, two other genes appear in this operon. First, the operon exhibits the *khtT* gene, which codes for an ancillary hydrophilic regulator protein (18.5 kDa, 165 amino acids per subunit). Interestingly, *khtT* only exhibits a partial RCK domain: only the RCK_C subdomain is present, at its C-terminal. Finally, the operon also contains *khtS;* which is still unclear whether this region codes for a 13 kDa, 112 amino acids protein or is a regulatory element of the operon.

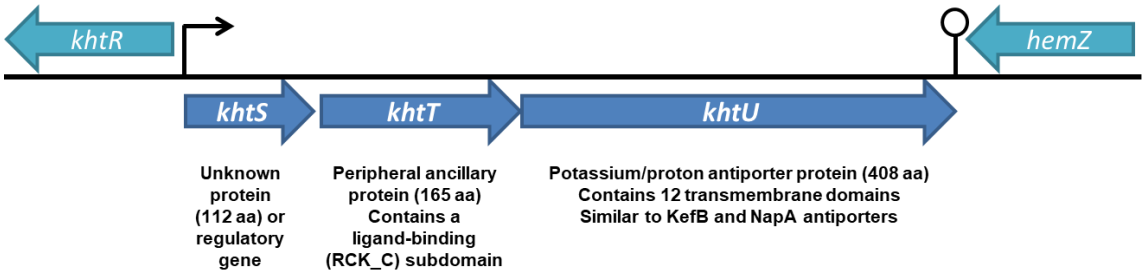

Figure 1.3 - Organization and schematic diagram of the *khtSTU* operon locus on the *Bacillus subtilis* chromosome. Adapted from SubtiList, the reference database for the *Bacillus subtilis* genome [37]

1.4. Current Knowledge of the KhtTU Transporter

The *khtSTU* operon was referenced in some studies on *B. subtilis'* transcriptomic which mention increased transcription in response to heat shock [39], alkaline stress [40], and cell wall stress [41]. Fujisawa et al. published a study [36] stating that the operon was upregulated during salt shock and alkali pH, which supports the idea that this protein is part of an osmotic and alkali stress response. Furthermore, it was suggested that both KhtT and KhtS are peripheral ancillary proteins and form a complex with KhtU regulating its activity. More recently, another study by the same group [35] proposed that the protein complex is composed solely by KhtT and KhtU and that the protein complex functions as a K^+/H^+ antiporter mechanism. The reasons behind the non-inclusion of KhtS were not specified. Using an antiport activity assay, they concluded that KhtU does not have antiporter activity when expressed alone, and that only the KhtTU complex is active. They also showed that activity of the KhtTU antiporter is dependent on pH, showing that activity is null at pH 7.5 and increases with alkaline pH, being highest at pH 9.0. Regarding the selectivity of KhtTU, their results reveal that Rb^+/H^+ antiport is also possible, while Na^+/H^+ or Li^+/H^+ antiport are not. Altogether, these results indicate that the KhtTU antiporter acts as a K^+/H^+ antiporter that is involved in adaptation to osmotic pressure (by exporting K^+) and alkaline stress (by importing H^+).

It has also been suggested that KhtTU is involved in methylglyoxal resistance in *Bacillus subtilis* [42]. Methylglyoxal is a toxic, endogenous by-product of glycolysis that damages DNA and proteins ultimately leading to cell death. In *E.coli* the Kef proteins (KefC and KefB) are involved in adaptation to exposure to toxic electrophiles, including methylglyoxal [43,44]. Increased K^+/H^+ antiport activity of Kef proteins by glutathione adducts, such as S-lactoyl-glutathione, causes cytoplasmic acidification, enhancing electrophile resistance and methylglyoxal detoxification [45,46]. As such, and due to the sequence similarity between KhtU and KefC it was suggested that KhtTU had a similar role in *B. subtilis*. Glutathione is absent in Gram-positive bacteria, instead bacillithiol (BSH) is the major reducing agent in *B. subtilis*. In parallel to the Kef systems of *E. coli*, it was proposed that KhtTU is activated by S-lactoyl-bacillithiol (SL-BSH), an intermediate formed during detoxification pathways [42]. However, this hypothesis lacks experimental evidence and there is still no proof that bacillithiol is capable of binding to KhtTU, let alone of activating it.

1.5. Cyclic di-AMP and K^+ homeostasis

Cyclic nucleotides that act as second messenger molecules play key roles in signaling pathways that sense environmental changes. The recently discovered cyclic di-AMP (c-di-AMP) (**Figure 1.4**) is an essential second messenger present in (but not limited to) Gram-positive bacteria such as *Bacillus subtilis* [47,48]. Intracellular concentrations between 2 and 5 µM have been measured in cytoplasmic extracts of this bacterium [49].

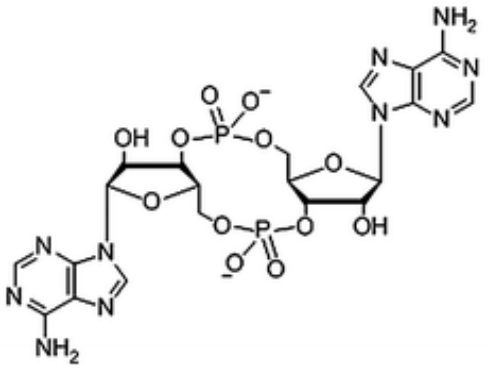

Figure 1.4 - Structural formula of a cyclic di-AMP molecule. Adapted from [50].

C-di-AMP is implicated in a variety of functions in the cell, including cell wall metabolism, DNA repair, sporulation, control of gene expression and potassium homeostasis [51]. Interestingly, c-di-AMP modulates potassium homeostasis by binding both proteins and RNA molecules. The *ktrAB* and *kimA* genes (responsible for expression of the high-affinity potassium uptake proteins mentioned in previous subchapters) are under the control of a riboswitch that responds to c-di-AMP, inhibiting transcription [52]. In fact, transcription of these genes is only possible at low intracellular c-di-AMP [52]. In addition, c-di-AMP acts as a ligand of the regulatory ancillary protein of the KtrAB system KtrA [53]. This protein assembles as a tetramer of dimeric RCK domains and c-di-AMP binds at the dimer interface [54]. This interaction between c-di-AMP and the RCK_C domain of KtrA in not limited to *B. subtilis*, being also found in *S. aureus*, *S. pneumoniae* or *C. glutamicum* [48]. Overall, this suggests that c-di-AMP has a role in controlling K^+ homeostasis, mostly through inhibiting its uptake beyond normal levels. Conversely, high levels of K^+ also increase c-di-AMP levels in the cell, suggesting that the system is bidirectionally regulated [52].

1.6. Importance of Studying Potassium Transporters

As disclosed in the previous sections, potassium transporters play an essential role throughout all domains of Life. In nerve and muscle cells of higher organisms, their crucial role in K^+ homeostasis implicates these proteins in the control of action potential frequency and duration, and ultimately in the regulation of neurotransmitter release and hormone secretion, epithelial electrolyte transport, cell proliferation, apoptosis, and tumor progression [55–58].

A relevant application of the knowledge acquired from potassium transporters is related to antibiotic resistance. Antibiotic resistance is a major healthcare problem and there is a pressing need to identify new antibacterial strategies [59]. The physiological importance of potassium homeostasis for the survival of bacteria together with the fact that the bacterial machinery that regulates potassium transport is biochemically different from the machinery in mammalians makes bacterial potassium transporters potential new targets for antibacterial strategies. Detailed characterization of the machinery is a crucial first step for the development of these strategies. In fact, investigation of regulatory proteins present in the Ktr or Trk systems has already shown potential in the study of antibiotic susceptibility in known pathogens such as *S.aureus* [60], *S. enterica* [61] or *M. smegmatis* [62], related to *M. tuberculosis.*

In conclusion, the biochemical and biophysical study of potassium transporters is of indisputable importance. Visualization of regulatory subunits and the analysis of their binding sites through crystallography would prove a valuable approach in exploring the modulation of transporter activity.

2. Objectives

The main goal for this work was to characterize the molecular properties of the KhtTU antiporter of *Bacillus subtilis* with particular emphasis on elucidating the role of regulatory protein KhtT. We were interested in answering such questions as: what is the molecular basis of the transporter activity and how is it regulated? If it is regulated by a ligand, what residues comprise its binding site? What is the architecture of the regulatory domain and what are the differences and similarities between KhtT and other RCK domains? What is the function of this antiporter in the potassium homeostasis machinery? Also, what explains its selectivity towards K^+? And is it involved in methylglyoxal detoxification through bacillithiol signaling?

Accordingly, the first sub-goal was to design and build an expression vector system for heterologous expression of all the proteins of the *khtSTU* operon and to determine the optimal expression and purification conditions for each protein. Also, since KhtT and KhtU are expected to act together, the optimization of a protocol for the expression of a KhtTU complex was also an objective.

Subsequently, two different approaches were taken in order to investigate the biochemical and biophysical properties of the KhtU antiporter and its regulatory component KhtT: the study of its functional properties (which consisted on ligand screening by differential scanning fluorimetry, followed by ligand affinity determination by calorimetry and characterization by antiporter activity assays) was complemented with the study of its structural properties (which consisted on attempting to obtain its three-dimensional structure through crystallography and x-ray diffraction).

3. Materials and Methods

3.1. Reagents, Growth Media and Competent Cells

Bacterial growth media was prepared according to **Table 3.1**; sterilization was achieved by autoclaving for 20 minutes at 121ºC. Information about the *E. coli* competent cell strains used in molecular biology or small and large-scale protein expression protocols in this work is displayed in **Table 3.2**. Bacillithiol (BSH) was purchased as $(BSH)_2$ 2xTFA salt from Vanderbilt Institute of Chemical Biology, Vanderbilt University, USA.

Table 3.1 - Composition of growth media used in cell cultures used throughout this work.

Lysogeny Broth (LB)	10 g/L Tryptone, 5 g/L Yeast Extract, 10 g/L NaCl
LB with K+ (LBK)	10 g/L Tryptone, 5 g/L Yeast Extract, 10 g/L KCl
Terrific Broth (TB)	20 g/L Tryptone, 24 g/L Yeast Extract, 0.4% Glycerol, 17 mM KH_2PO_4, 72 mM K_2HPO_4
2xYT	16 g/L Tryptone, 10 g/L Yeast Extract, 5 g/L NaCl, pH 7.0

Table 3.2 - Genotype information of the *E. coli* strains used throughout this work.

DH5α	F– endA1 glnV44 thi-1 recA1 relA1 gyrA96 deoR nupG purB20 φ80dlacZΔM15 Δ(lacZYA-argF)U169, hsdR17(rK–mK+), λ–
XL1-Blue	recA1 endA1 gyrA96 thi-1 hsdR17 supE44 relA1 lac [F´ proAB laclq ZΔM15 Tn10 (Tetr)]
BL21 (DE3)	F- ompT lon hsdSB (rB-mB-) gal dcm (DE3)
Rosetta™	F- ompT hsdSB(rB- mB-) gal dcm (DE3) pRARE (CamR)
B834 (DE3)	F^- ompT $hsdS_B(r_B^- m_B^-)$ gal dcm met (DE3)
KNabc	Derivative of TG1 cells (ΔnhaA, ΔnhaB, ΔchaA)

3.2. Molecular Biology

All DNA constructs (see **Table 3.3**) were created using traditional molecular biology techniques. Insert amplification was performed by using 25-30 cycles of polymerase chain reaction (PCR) with *Bacillus subtilis* genomic DNA, the oligos shown in the table, and either Pfu or Exact Run DNA polymerases (Thermo Scientific). PCR products were then digested for 2 hours at 37ºC using the appropriate restriction enzymes, as were their respective vectors. Digestion was followed by gel purification and a ligation reaction incubating T4 DNA Ligase and both digests at 4ºC overnight. Ligation reactions were then transformed into DH5α or XL1-Blue cells and plated onto LB-agar plates with the appropriate antibiotic. 3-4 colonies of each plate were selected, inoculated in 5-10 mL of liquid LB with antibiotic and grown at 37ºC, 225 rpm overnight. A second PCR reaction was performed on each culture to determine whether cloning had been successful. DNA from 2 positive clone cultures was extracted using NZYTech's MiniPrep Kit and sent to sequencing (GATC Biotech, Germany).

Table 3.3 - ***Primers and templates used to prepare the vectors used in biochemical studies on KhtT, KhtU, KhtS and KhtTU.***

Construct name:	Vector:	Insert:	Tags:	Oligos:
pRSFDuet:*khtU* **(NCBI Gene ID: 939761)**	pRSFDuet	**khtU On MCS 1**	N-terminal: His_6-Thr*	Forward: *(BamHI)* 5'–TAGCAGGATCCACTGGTGCCGCGCGGCAGCGGGGTGAGCCCGATGGAC-3' Reverse: *(NotI)* 5' – GAACTGCGGCCGCTCATCCCTGTTTTTTTGC -3'
pRSFDuet:*khtT* **(NCBI Gene ID: 936284)**	pRSFDuet	**khtT On MCS 1**	N-terminal: His_6-Thr*	Forward*: (BamHI)* 5' – TAGCGGGATCCACTGGTGCCGCGCGGCAGCGGGTTGAATATTAAAG-3' Reverse*: (NotI)* 5' – GTTAAGCGGCCGCTCACACGCCCTCTCC – 3'
pRSFDuet:*khtS* **(NCBI Gene ID: 939291)**	pRSFDuet	**khtS On MCS 2**	None	Forward: *(NdeI)* 5' – TAGCGCATATGGGGAGAAGGGAGGAAAGGAAC – 3' Reverse: *(XhoI)* 5' – TAGGTCTCGAGTCATATTCGGAGGTAATTAG – 3'
pRSFDuet:*khtT+khtS*	pRSFDuet:khtT	**khtS On MCS 2**	khtT N-terminal: His_6-Thr*	Forward: *(NdeI)* 5' – TAGCTCATATGGTGGTTCTGCCTTCCCAGTTTG – 3' Reverse: *(XhoI)* 5' – TAGGTCTCGAGTCATATTCGGAGGTAATTAG – 3'
pRSFDuet:*cytS***	pRSFDuet	**cytS On MCS 2**	None	Forward: *(NdeI)* 5' – TAGCTCATATGGTGGTTCTGCCTTCCCAGTTTG – 3' Reverse: *(XhoI)* 5' – TAGGTCTCGAGTCATATTCGGAGGTAATTAG – 3'
pET15b:*cytS***	pET15b	**cytS**	N-terminal: His_6-Thr*	Forward: *(NdeI)* 5' – TAGCTCATATGGTGGTTCTGCCTTCCCAGTTTG – 3' Reverse: (*BamHI)* 5' - TAGGTGGATCCTCATATTCGGAGGTAATTAGAC – 3'
pRSFDuet:*khtU+khtT*	pRSFDuet:khtU	**khtT On MCS 2**	khtU N-terminal: His_6-Thr*	Forward: *(NdeI)* 5' – TAGCTCATATGAATATTAAAGAAAACGATCTGC – 3' Reverse: *(XhoI)* 5' – TAGCGCTCGAGTCACACGCCCTCTCCAGAAAGAAAATCG – 3'
pET24dT:*khtTU*	pET24dT***	**khtTU**	khtU C-terminal: Thr*-His_6	Forward: *(NcoI)* 5' – TAGCTCCATGGGGAATATTAAAGAAAACGATCTGC – 3' Reverse: *(XhoI)* 5' – TAGGTCTCGAGTCCCTGTTTTTTTGCGGGCTG – 3'
pQE-60:*khtTU*	pQE-60	**khtTU**	None	Forward: *(NcoI)* 5' – TAGCTCCATGGGGAATATTAAAGAAAACGATCTGC – 3' Reverse: (NotI) 5' – TAGGTAGATCTTCATCCCTGTTTTTTTGCGGGCTG – 3'

* "Thr" symbolizes a thrombin cleavage site (nucleotide sequence CTGGTGCCGCGCGGCAGC, coding for the amino acid sequence LVPR↓GS, recognized by this protease) embedded in the oligo, to be placed between the polyhistidine tag and the protein sequence.

** "cytS" is the name chosen to designate the 84-aminoacids long segment between amino acids 29 and 112 of khtS, believed to be a hydrophilic, cytosolic part of KhtS, according to structure prediction tools and by previous studies [36].

*** This vector derives from pET-24d but contains a thrombin cleavage site between the stop codon and the polyhistidine tag.

3.3. Small-scale Protein Expression Tests

Protein expression levels for each construct were tested by changing a number of variables: Use of different *E. coli* strains [BL21(DE3) or Rosetta (strain that supplies extra tRNAs)]; Different growth media [Lysogeny Broth (LB), 2xYT, Terrific Broth (TB), see media composition in section 3.1.]; Different times and temperatures of induction [3 hours at 37ºC or overnight at 20ºC (the latter with induction of heat and cold-shock chaperones by 1% ethanol and ice-bath treatment, respectively]. Induction started by addition of 0.5 mM of isopropyl-β-D-1-thiogalactopyranoside (IPTG).

In the case of cytosolic proteins/domains, small-scale expression tests were performed by inoculating 50 mL of liquid media (containing antibiotic) with a resuspension of transformed colonies followed by whatever set of conditions being tested. In the end, cells were pelleted, resuspended in 1 mL of Expression Test Lysis Buffer (50 mM Tris-HCl pH 8.0; 150 mM KCl; 2.5 mM DTT in the presence of protease inhibitors, DNAse and lysozyme) and lysed by sonication cycles (Branson sonifier 250; 3-4 cycles of 15 seconds each, power level 3, duty cycle of 30%). After collecting samples of total extract (TE) (just after sonication) and supernatant (S) (after a 30 min, 12000 g centrifugation of the lysates) fractions, soluble protein levels of expression were assessed by SDS-PAGE. In the case of construct pET15b:cytS, protein levels were also visualized by Western Blotting, using a Mouse-α-His as primary antibody, a horseradish peroxidase conjugated Goat-α-Mouse as secondary antibody and the enhanced chemiluminescence (ECL) reagent method.

In the case of membrane proteins, small-scale expression tests were performed by inoculating 1 L of liquid media (containing antibiotic) with a resuspension of transformed colonies followed by growth until the OD_{600nm} of the culture reached 1.0-1.1. At that point, protein expression was induced and after each induction period the cells were pelleted, resuspended in Membrane Protein Expression Test Lysis Buffer (50 mM HEPES pH 8.0; 210 mM NaCl; 90 mM KCl; 5 mM Imidazole pH 8.0 in the presence of protease inhibitors) and lysed using a prechilled cell cracker (Emulsiflex-C5 – Avestin). Extraction and solubilization of membrane proteins was done by adding 20 mM of n-Dodecyl-β-D-maltoside (DDM) and 5% glycerol to the lysates, followed by overnight rocking at 4ºC. The next day, lysates were centrifuged for 45 mins (25000 g at 4ºC) and the soluble fraction was loaded into an EconoPak column containing 1 mL of preequilibrated Ni^{2+} affinity bead resin. After washing the beads with 5 CVs of Wash Buffer (50 mM HEPES pH 8.0; 210 mM NaCl; 90 mM KCl; 5% Glycerol; 1mM DDM and 20 mM Imidazole pH 8.0;), the membrane protein of

interest was eluted using increasing amounts of Imidazole in Elution Buffer (25 mM HEPES pH 8.0; 140 mM NaCl; 60 mM KCl, 5% Glycerol; 1mM DDM and 50-500 mM Imidazole pH 8.0). Expression levels for each construct were then assessed by SDS-PAGE and Western Blotting using Mouse-α-His as primary antibody, a horseradish peroxidase conjugated Goat-α-Mouse as secondary antibody and visualization by the enhanced chemiluminescence (ECL) reagent method.

3.4. Pull-down Assay of KhtT and KhtS

His-tagged KhtT was used as bait protein in a pull-down assay performed while testing for KhtS expression using the pRSFDuet:*khtT+khtS* construct. The pull-down assay was done using Millipore PureProteome™ Nickel Magnetic Beads. The protocol consisted on incubating approximately 1 mL of the lysates obtained in co-expression tests of KhtT and KhtS (section 3.3.) with 25 µL of nickel magnetic bead slurry pre-equilibrated with Tris-buffered saline (TBS) for 1 hour on a rotating mixer, at room temperature. Beads and supernatant were separated using the magnetic properties of the beads and a PureProteome™ Magnetic Stand. After removing the unbound fraction and washing the beads 5 times with 500 µL of TBS supplemented with 20 mM Imidazole, the beads were resuspended with 50 µL SDS-PAGE sample buffer, boiled for 5 minutes and loaded on an SDS-PAGE gel for analysis.

3.5. KhtT Expression and Purification Protocol

3.5.1. Native KhtT

The standard protocol used for large-scale native KhtT expression and purification used throughout this work consisted on the steps that follow: *E. coli* BL21(DE3) competent cells were transformed with pRSFDuet:*khtT* expression vector and plated onto LB plates containing 50 µg/mL kanamycin. The next day, all colonies of the plate were resuspended, inoculated into 1 L of liquid LB (with 50 µg/ml kanamycin) grown at 37ºC, 160 rpm in an orbital shaker until OD_{600nm} reached 0.8, at which point cells were induced with 0.5 mM IPTG and incubated 3 h further. Induced cultures were then pelleted at 3000 g for 20 minutes at 4ºC and stored at -20 ºC.

Cell lysis was performed by resuspending the cells in KhtT Lysis Buffer (50 mM Tris-HCl pH 8.0; 150 mM KCl) followed by cell cracking using a prechilled Emulsifex-C5 (Avestin). Unwanted proteolytic digestion was inhibited by adding 1 mM phenylmethylsulfonyl fluoride (PMSF), 1 µg/mL Leupeptin and 1 µg/mL Pepstatin A to the cell homogenate. Crude cell extract was then clarified by centrifugation (45 minutes at 25000 g, 4ºC). Supernatant fraction was collected, incubated with preequilibrated NiNTA beads rocking for 90-120 minutes at 4ºC and loaded on a column. Beads were then washed with 10xCV of Wash Buffer (50 mM Tris-HCl pH 8.0; 300 mM KCl; 10 mM Imidazole), His-tagged KhtT was eluted by addition of Elution Buffer (50 mM Tris-HCl pH 8.0; 150 mM KCl; 50 mM Imidazole) and the amount of protein obtained was estimated by reading the absorbance of the eluate at 280nm, using a molar extinction coefficient [ε(KhtT monomer) = 9970 M^{-1} cm^{-1}] predicted by the ProtParam software, a tool from ExPASy's resource portal. His-tagged KhtT protein fraction was then dialyzed overnight against KhtT Dialysis Buffer (20 mM Tris-HCl pH 8.0; 150 mM KCl in a volume ratio of 1:100 to 1:200) in the presence of 1-2 µg of Bovine Alpha Thrombin per mg of KhtT protein in order to cleave off the polyhistidine tag. The following day, dialyzed fraction was loaded onto a second preequilibrated NiNTA bead column to further select only untagged KhtT. Protein fraction was then concentrated using PALL or VivaSpin concentrators and injected in a preequilibrated size-exclusion chromatography Superdex 200 10/300 GL column (GE Healthcare) after passing through a 0.22 µm filter. Fractions containing pure KhtT were then pooled together and a final protein fraction was obtained in KhtT Buffer (20 mM Tris-HCl pH 8.0; 150 mM KCl). Small fractions were kept throughout the whole process for SDS-PAGE analysis.

3.5.2. Selenomethionine Variant of KhtT

The expression of a selenomethionine (SeMet) variant of KhtT was done using *E. coli* B834(DE3) (a methionine auxotroph strain) and Molecular Dimension's SelenoMet™ commercial kit, which consisted in growing the cells in a synthetic M9 minimal media supplemented with glucose, vitamins and all the amino acids with the exception of L-methionine. To this media 4 mL of a 10 mg/mL L-Selenomethionine stock (from the kit) were added per liter of culture. From this point forward the expression and purification protocol was exactly the same as with the native KhtT, with the addition of 1 mM TCEP to every buffer as a reducing agent being the only difference.

3.6. KhtTU Expression and Purification Protocol

The standard large-scale protocol for KhtTU complex expression and purification developed in this work consists on the following steps: *E. coli* BL21(DE3) competent cells were transformed with pET24dT:*khtTU* expression vector and plated onto LB plates containing 50 µg/mL kanamycin. The next day, all colonies of the plate were resuspended, inoculated into 1 L culture flasks with liquid 2xYT (with 50 µg/ml kanamycin) and grown in an orbital shaker at 37ºC, 160 rpm until OD_{600nm} reached 1~1.1, at which point cells were induced with 0.5 mM IPTG and incubated 3 h further. Induced cultures were then pelleted for 20 mins at 3000 g, 4ºC and stored at -20 ºC.

Pellets were resuspended in KhtTU Lysis Buffer (50 mM HEPES pH 8.0; 100 mM NaCl; 50 mM KCl; 10 mM Imidazole pH 8.0) followed by cell cracking using a prechilled Emulsifex-C5 (Avestin). Unwanted proteolytic digestion was inhibited by adding 1 mM PMSF, 1 µg/mL Leupeptin and 1µg/mL Pepstatin A to the cell homogenate. At this point, 20 mM DDM and 5% glycerol were added to the lysate, which was then left rocking overnight at 4ºC for extraction of cellular membranes. The following day, the lysate was centrifuged (45 minutes, 25000 g, 4ºC) and the supernatant was loaded into a preequilibrated nickel affinity purification column. The flow-through was reloaded into the column to increase the probability of binding. Beads were then washed with 10xCV of Wash Buffer (50 mM HEPES pH 8.0; 210 mM NaCl; 90 mM KCl; 5% Glycerol; 1 mM DDM; 20 mM Imidazole pH 8.0) and bound KhtTU complex was eluted using Elution Buffer (25 mM HEPES pH 8.0; 140 mM NaCl; 60 mM KCl; 5% Glycerol; 1mM DDM; 150 mM Imidazole pH 8.0). Protein fraction was immediately diluted 1:5 in Elution Buffer without imidazole to reduce protein aggregation and dialyzed against KhtTU Dialysis Buffer (25 mM HEPES pH 8.0; 140 mM NaCl; 60 mM KCl; 5% Glycerol; 1mM DDM) in the presence of 1 µg of Bovine Alpha-Thrombin / mg protein. As with KhtT, protein amount was estimated by reading the absorbance of the eluate at 280 nm and using a predicted molar extinction coefficient [ε(KhtTU monomers) = 31400 M^{-1} cm^{-1}]. The following day, dialyzed protein was concentrated and injected in a preequilibrated size-exclusion chromatography Superdex 200 10/300 GL column (GE Healthcare). Fractions containing KhtTU protein complex in final KhtTU buffer (25 mM HEPES pH 8.0; 140 mM NaCl; 60 mM KCl; 1mM DDM) were pooled together, concentrated and re-dialyzed to reduce detergent levels to a minimum.

3.7. Ligand Testing by Thermal Shift Assay

The thermal denaturation temperature of purified native KhtT was studied both with the absence and presence of potential ligands, in an attempt to identify ligands of this protein. Each sample consisted of a final concentration of 3 μM pure KhtT (in KhtT Buffer: 50 mM Tris pH 8.0; 150 mM KCl), a 2.5 X final concentration of Sypro Orange Protein Gel Stain and the final concentration of each ligand being tested varied between 0.1 mM and 10 mM. The total volume of each sample was either 40 or 50 μL. The experiment was then setup in a 96-well PCR White Plate (Bio-Rad) and performed in a iQ5 real-time PCR system (Bio-Rad) using the Cy3 filter specific for Sypro Orange detection (λex = 490 nm / λem = 575 nm), with the temperature varying from 25 ºC to 95 ºC in 0.5 ºC increments of 30 seconds each. Data was then analyzed using the CFX Manager Software (Bio-Rad).

C-di-AMP and c-di-GMP were obtained from BioLog in powder form and solutions were prepared by resuspension in 100 mM Tris-HCl pH 8.0. Reduced BSH was obtained by resuspending the salt in 20 mM HEPES-NaOH pH 7.5 and 2 mM TCEP. Oxidized BSH was obtained by overnight incubation of the reduced form with 10 mM N-ethylmaleimide, an alkylating reagent reactive towards thiols, rendering ethylmaleimide-bacillithiol (E-BSH). The resulting products were not evaluated.

3.8. Isothermal Titration Calorimetry (ITC)

Preparation of KhtT prior to ITC was done as described in section 3.5, with the addition of a second dialysis step the day before the assay was performed, against ITC Dialysis Buffer (50 mM HEPES pH 8.0; 150 mM KCl). Dialyzed protein was then centrifuged (30 minutes at 12000 g, 4ºC) to remove any possible aggregates and the ligands being tested (either c-di-AMP or c-di-GMP) were prepared by diluting stock aliquotes in ITC Dialysis Buffer. 3 subsets of experiments were performed: The first consisted on 20 or 30 μM KhtT samples in the cell titrated with 150 or 300 μM ligand samples in the syringe, respectively. The second subset consisted on a reverse titration: samples of 6 μM ligand in the cell were titrated with 175 μM KhtT set in the syringe. The last set of experiments consisted on control samples: ITC Dialysis Buffer in the cell and 300 μM ligand samples in the syringe, for reference.

Each experiment was executed in a MicroCal VP-ITC calorimeter (GE Healthcare), using 2 mL of cell sample volume and 500 μL of syringe sample volume, at 25 ºC (unless otherwise noted). Data were visualized and analyzed with Origin 7 Software (by OriginLab) and with AFFINImeter ITC Data Analysis Software [by Software for Science Developments (S4Sd)] using a single binding site model.

3.9. Controlled Proteolysis Assay

The effect of c-di-AMP on KhtT's proteolytic pattern was assessed by a controlled proteolysis assay. 15 µL samples containing 15 µg (50 µM) of pure protein were digested with commercial proteases (Trypsin, Chymotrypsin) at different protease-to-protein ratios (1:50; 1:100; 1:500; 1:1000) for 1 hour at room temperature in the absence or presence of 50 µM c-di-AMP. The reaction was stopped with the addition of SDS sample buffer followed by boiling and each sample was loaded onto a 17% SDS-PAGE gel for analysis of the digestion patterns.

3.10. KhtTU Everted Vesicles and Antiporter Activity Assay

Everted vesicles containing KhtTU antiporter were prepared by growing KNabc cells (a K^+/H^+, Na^+/H^+ and Ca^+/H^+ antiporters deficient *E. coli* strain) previously transformed with pQE60:*khtTU* in liquid LBK media (supplemented with 100 µg/mL ampicillin) until OD_{600nm} reached 0.9-1.0, at which point cultures were induced with 0.5 mM IPTG, incubated at 37ºC for 3 hours and pelleted by a 20 minutes, 3000 g centrifugation. The cell pellet was then resuspended in minimum volume of Vesicle Lysis Buffer (10 mM Tris-HCl pH 8.0; 140 mM Choline Chloride, 0.5 mM DTT and 250 mM Sucrose), pelleted again and weighed. Cells were then resuspended in Vesicle Lysis Buffer and lysed by passage through a French Press at a pressure of 4000 psi in the presence of DNAse and 5 mM $MgCl_2$. Unbroken cells were pelleted by two sequential centrifugations of 15 min at 10000 g. Everted vesicles were extracted from the spin-cleared lysate by 1 hour centrifugation at 100.000 g, with the resulting pellet being resuspended once, washed and pelleted again. Vesicle pellet was resuspended in 1 mL Vesicle Lysis Buffer per gram of original wet cell weigh, total protein concentration was estimated using Bradford reagent method using bovine serum albumin (BSA) as standard and vesicles were stored in small aliquotes at -80ºC. The same protocol was applied using an empty pQE-60 vector in order to obtain vesicles without the antiporter as a negative control.

To perform the assay, vesicles were diluted in Vesicle Assay Buffer (15 mM Tris-HCl pH 8.5; 140 mM Choline Chloride; 5 mM $MgCl_2$). Each sample contained approximately 200 µg of total protein in a volume of 2 mL. 9-Amino-6-Chloro-2-Methoxyacridine (ACMA) was used as a fluorescence probe to quantify changes in transmembrane proton gradient; ACMA was added at a final concentration of 2 µM

seconds before running the assay. Fluorescence was measured using a HORIBA Fluoromax-4 cuvette spectrofluorometer with constant stirring settings and excitation and emission wavelengths of 410 nm and 480 nm respectively. An integration rate of 0.2 seconds and a 2-nm slit were selected. A respiration-generated pH gradient was generated by addition of 4 mM D-Lactate, resulting in a quenching in ACMA fluorescence. KhtTU antiporter activity was studied by addition of a salt (KCl, RbCl or NaCl) and generation of a monovalent cation gradient. The effect of c-di-AMP and c-di-GMP on the function of KhtTU was studied by addition of the ligand to the sample cuvette seconds before the salt was added, initiating the antiporter activity. The effect of reduced bacillithiol (BSH) and its oxidized form (E-BSH) was also tested in this experiment. All assays were performed in triplicates and at room temperature. All curves were fitted with single or double exponentials using GraphPad Prism software.

3.11. Crystallography

Initial crystallization screens for native KhtT were performed using purified protein at a concentration of 8-10 mg/mL in KhtT buffer (20 mM Tris-HCl pH 8.0; 150 mM KCl), centrifuged for 30 minutes at 12000 g at 4ºC in a table-top centrifuge to clear any aggregates, and the following commercial screens: JBScreen Basic, JBScreen JCSG++ HTS L (Jena Biosciences); Morpheus, Wizard I&II, PACT Premier, MIDAS (Molecular Dimensions), Nextal Classics L Suite and Nextal Classics II Suite (QIAGEN). When testing or using the effect of a ligand, the same was added to the protein fraction and left incubating on ice for 30 minutes before setting up the plates.

Each initial screening drop consisted on 0.6 µL drops (0.3 µL protein + 0.3 µL reservoir solution) and 40 µL of reservoir solution and incubated at 4ºC and 20ºC. Any crystal-generating condition was optimized by fine tuning around each component of said condition (handmade screens varying precipitant concentrations, pH, drop size, protein-to-reservoir ratio; see Appendix, **Table 8.3** and **Table 8.4**) and handmade screens were set up in 48-well plates with a drop size of 2 µL (1 µL protein + 1 µL reservoir solution) with 150 µL reservoir solution volume. Drops were set up using the sitting drop method with a protein crystallization robot (Oryx 4 by Douglas Instruments).

The selenomethionine variant of KhtT was crystallized using the same handmade screens around hit conditions successfully used for native KhtT, in the exact same conditions. Heavy atom soaking of native KhtT crystals was performed by transferring them to a new replica drop with addition of 1 mM Heavy Atom Solution to the drop (description of each stock in Appendix, **Table 8.2**) followed by overnight incubation.

Native KhtT, SeMet-KhtT and heavy atom-soaked KhtT crystals were prepared for data acquisition by transferring them to cryoprotectant solutions with increasing percentage of cryoprotecting agent (up to 25% glycerol, ethylene glycol or PEG400) and ultimately flash-freezing them in liquid nitrogen. Data acquisition was done by lab colleagues at the Soleil Synchrotron in Paris, France at either the Proxima I or Proxima II beamlines.

3.12. Cyclic-di-AMP Binding Site Comparison

A three-dimensional model for the RCK_C domain of KhtT was obtained using Swiss-Model [63], a protein structure homology-modelling server and the structure of the RCK domain of MthK, a K^+ channel from *M. thermoautotrophicus* [28] (PDB code: 4L74), as a template. This model was then compared with the structure of the RCK_C domain of KtrA of *S. aureus* bound to c-di-AMP [54] (PDB code: 4XTT), in order to try to estimate which residues may constitute the binding site in KhtT. The mapping of the residues that formed hydrogen bonds between c-di-AMP and the residues of each protein was done and visualized with PyMOL. A pairwise sequence alignment between KhtT and KtrA of *S. aureus* was also done via the Clustal Omega (EMBL-EBI) sequence alignment tool.

4. Results & Discussion

4.1. Protein Expression and Purification

The first step in characterizing the biochemical and biophysical properties of the proteins involved in the *khtSTU* operon was to determine and optimize the conditions for large-scale expression and purification.

4.1.1. KhtT Expression and Purification

The best conditions for expression of soluble KhtT were tested as described in section 3.3. In short, the general strategy was growing different transformed *E. coli* strains in different media, temperature and/or induction periods. After growing the cells in different conditions, the level of soluble protein expression was assessed by SDS-PAGE analysis (**Figure 4.1**).

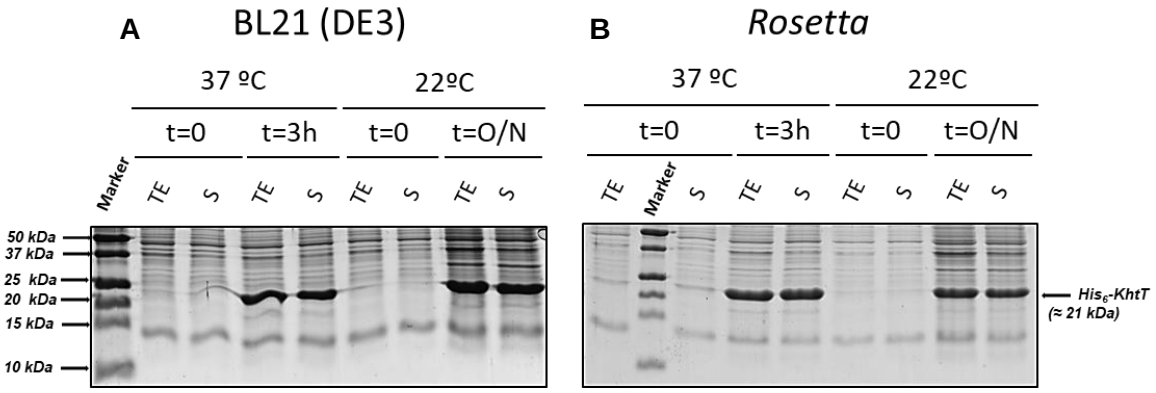

Figure 4.1 - SDS-PAGE gels of KhtT expression tests in (A) BL21(DE3) and (B) Rosetta *E.coli* strains. Cells were lysed by sonication and centrifuged. Pre-centrifugation Total Extract (TE) and post-centrifugation supernatant (S) samples were then loaded on a 17% SDS-PAGE gel and stained with NZYTech's BlueSafe gel stain. Molecular weight protein markers are indicated on the left (Bio-Rad's Precision Plus Protein™ All Blue Prestained Protein Standards); the expected position of His-tagged KhtT is marked on the right. Legend for each lane is displayed above each gel.

The gels show that KhtT is produced in both *E. coli* strains as a soluble protein in apparently large quantities regardless of time of induction. As such, the simplest conditions were selected to work with: 3 hours of induction at 37ºC. Large-scale expression and purification was then optimized, ultimately being standardized as described in section 3.5. The outcome of the first steps of KhtT purification protocol, consisting on cell lysis, lysate centrifugation, immobilized metal affinity chromatography (IMAC) using nickel beads and thrombin digestion are shown in **Figure 4.2**. Digested KhtT was then further purified using size exclusion chromatography; the chromatogram obtained is shown in **Figure 4.3**, together with a gel analysis of the peak fractions.

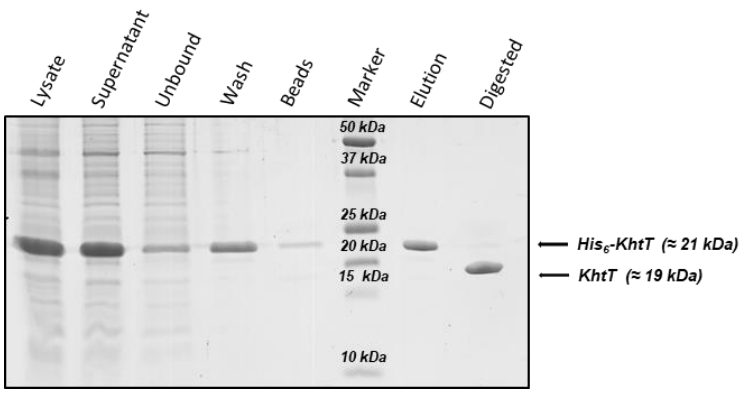

Figure 4.2 - SDS-PAGE gel of the overall extraction and purification protocol for KhtT. A spin-cleared cell extract supernatant was loaded in an IMAC column; the beads were washed with 10 mM Imidazole and protein eluted with 50 mM Imidazole. Overnight dialysis in the presence of thrombin yielded a fraction of tagless KhtT. Arrows to the right mark the expected position of His-tagged KhtT or digested KhtT. Legend for each lane is displayed above the gel.

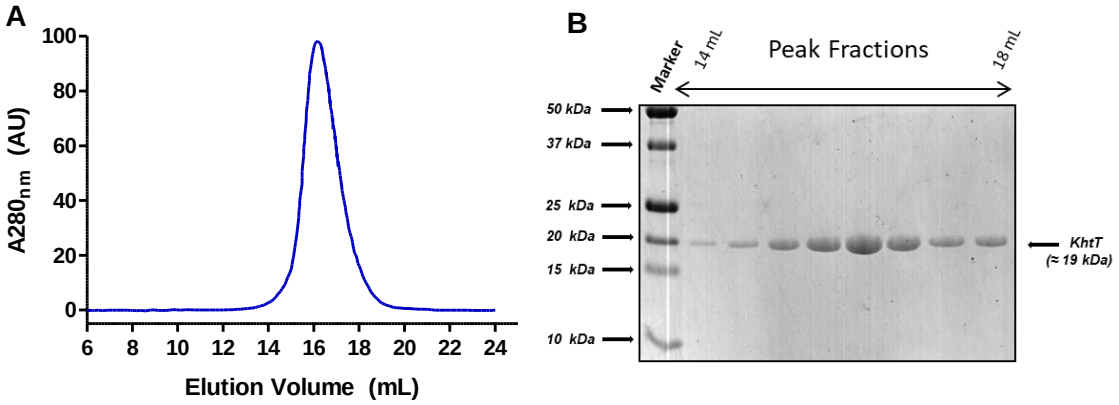

Figure 4.3 - (A) Chromatogram of KhtT size exclusion chromatography and (B) SDS-PAGE gel of peak fractions. Protein peak elutes at approximately 16 mL of elution volume in the Superdex 200 10/300 GL column. The chromatogram also shows that there are no aggregates in the void volume (8 mL). Samples from each peak fraction (approximately 0.5 mL each) were loaded on a 17% SDS-PAGE gel and stained with NZYTech's BlueSafe gel stain. Arrows to the left indicate protein markers (Bio-Rad's Precision Plus Protein™ All Blue Prestained Protein Standards) and arrow to the right marks the expected position of KhtT in each lane.

KhtT's size exclusion chromatography profile shows a single sharp peak suggesting that the protein is stable and monodisperse in the conditions used. There is no aggregate in the void volume (8 mL) and no other peak is observed (no contaminants). The comparison of the peak elution volume (16 mL) with a previously determined calibration curve for this column (see Appendix, **Figure 8.1**) allows an estimation of the oligomeric state of the protein. The apparent molecular weight is 38 kDa, corresponding to a dimer.

The protocol for expression and purification of KhtT yields approximately 10 mg of pure and well behaved protein per liter of culture.

4.1.2. KhtS Expression Testing

Expression tests for KhtS followed a slightly different approach. The double gene expression vector pRSFDuet:*khtT*+*khtS* was constructed for two reasons: first, since KhtS is coded in a separate promoter, its levels of expression could be assessed as in an individual construct. The second reason is that since this vector simultaneously codes for His_6-tagged KhtT on one promoter and tagless KhtS on the other, the hypothesis of an eventual complex formation by both proteins could also be tested by a pull-down assay (by binding KhtT to a bead resin and visualizing the proteins existing on the eluted fraction). Conditions for expression of KhtS using this construct were tested as shown above for KhtT. Soluble protein levels for each condition tested were assessed by SDS-PAGE (**Figure 4.4**).

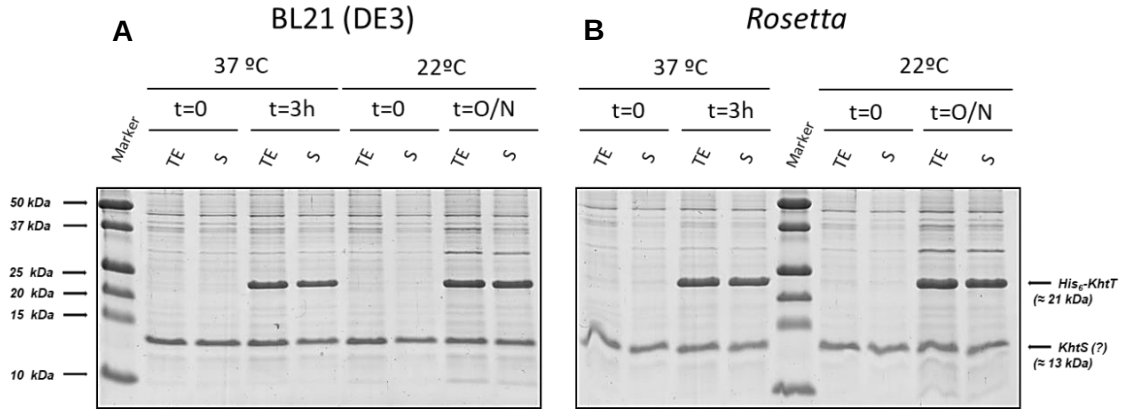

Figure 4.4 - SDS-PAGE gels of KhtS expression and KhtT co-expression tests in (A) BL21(DE3) and (B) Rosetta *E. coli* strains. Cells were lysed by sonication and centrifuged. Pre-centrifugation total extract (TE) and post-centrifugation supernatant (S) samples were then loaded on a 17% SDS-PAGE gel and stained with NZYTech's BlueSafe gel stain. Molecular weight protein markers are indicated on the left (Bio-Rad's Precision Plus Protein™ All Blue Prestained Protein Standards); the expected positions of His-tagged KhtT and KhtS are marked on the right. Legend for each lane is displayed above each gel.

As expected, KhtT was expressed in high soluble quantities. On the other hand, it was not possible to observe an induced 13 kDa band corresponding to KhtS. There is a 13 kDa protein that appears in all conditions, prior and after induction. It is likely that this is a contaminant that could conceal a modest level of expression of KhtS. As such, a pull-down assay (**Figure 4.5**) using the lysates from the expression tests was performed as a way to clarify this uncertainty and to simultaneously test if KhtS can form a complex with KhtT.

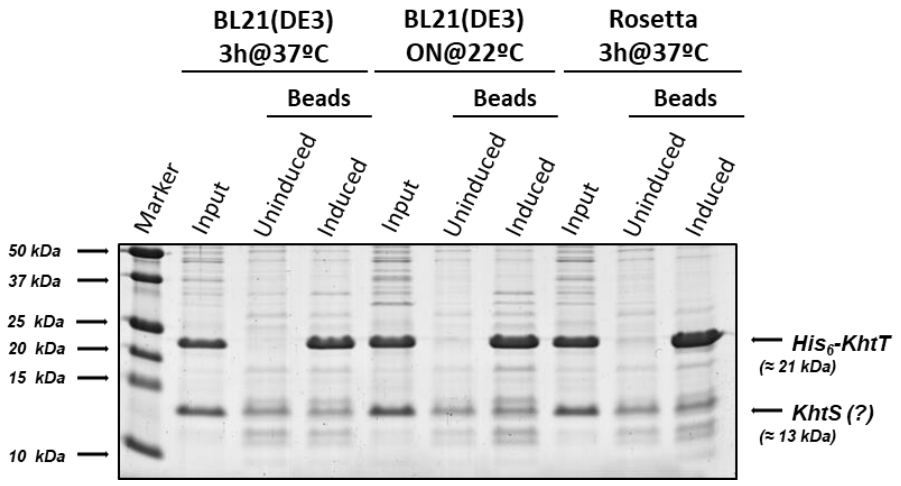

Figure 4.5 - SDS-PAGE gel of His_6-tagged KhtT and KhtS co-expression pull-down assay. 3h and ON lysates obtained from BL21(DE3) expression tests as well as ON lysates from Rosetta expression tests were incubated with magnetic nickel affinity beads. After removing the unbound fraction and washing, the beads were resuspended in sample buffer, boiled and loaded in the gel. For each growth condition the gel shows 3 samples: **Input** – loading of induced lysate samples obtained after the small-scale purification protocol; **Uninduced** – Result of the pull-down assay for uninduced lysate samples; **Induced –** Result of the pull-down assay for induced lysates. The arrows to the left mark the molecular weight of each protein marker (Bio-Rad's Precision Plus Protein™ All Blue Prestained Protein Standards) and the arrows to the right mark the expected position of His-tagged KhtT or KhtS in each lane.

His-tagged KhtT is clearly present in the pull-down bead samples of induced lysates, which means that the pull-down was successfully performed. However, there is no clear KhtS band in none of the samples and the fact that 13kDa contaminant levels are the same in both uninduced and induced samples suggests that KhtS was either unable to bind to KhtT or non-expressed at all. As such, the results suggest that KhtS is not significantly expressed in any of these expression test samples, since there is no distinction between uninduced and induced samples after the pull-down assay. Of course, this assay was based on the assumption that KhtS binds to KhtT and that may not be the case. The fact that throughout both assays (SDS-PAGE visualization of KhtS expression tests and KhtT + KhtS pull-down assay) the 13 kDa molecular weight band remains unchanged suggests that KhtS is most likely not expressed, at least not in the quantity needed for the remaining assays.

A different KhtS-related construct (pET15b:*cytS*) was tried as a final attempt to obtain KhtS. Previous studies [36], based on bioinformatics and structure-prediction tools, suggested that KhtS might be composed by a membrane-bound N-terminal and a cytosolic C-terminal. Therefore, a construct coding for an 84-aminocids long segment of KhtS, residues 29 to 112, believed to be the cytosolic part of the protein (hence the name "*cytS*"), was built and its expression was tested as before. In this construct the protein is N-terminally His_6-tagged and has an expected molecular weight of 11 kDa.

The visualization of expression tests results for this construct by SDS-PAGE and Western Blotting are shown in **FiguresFigure 4.6** and **Figure 4.7**.

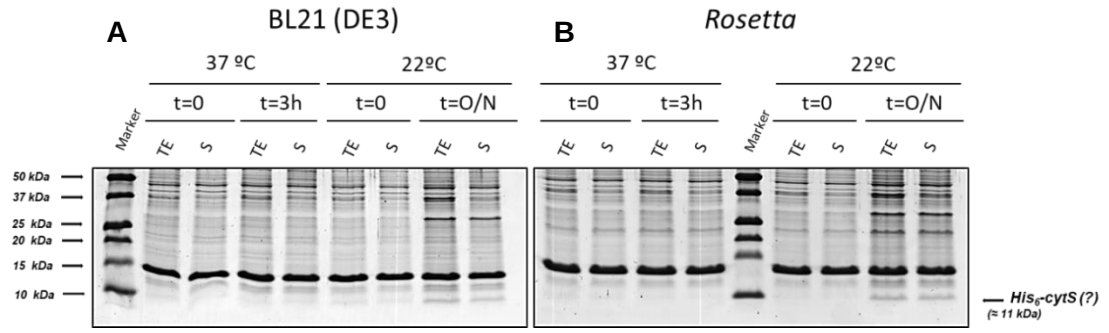

Figure 4.6 - SDS-PAGE gels of His-tagged cytS expression tests in (A) BL21(DE3) and (B) Rosetta *E. coli* strains. Cells were lysed by sonication and centrifuged. Pre-centrifugation Total Extract (TE) and post-centrifugation supernatant (S) samples were then loaded on a 17% SDS-PAGE gel and stained with NZYTech's BlueSafe gel stain. The arrows to the left mark the molecular weight of each protein marker (Bio-Rad's Precision Plus Protein™ All Blue Prestained Protein Standards) and the arrow to the right marks the expected position of His-tagged cytS. Legend for each lane is displayed above each gel.

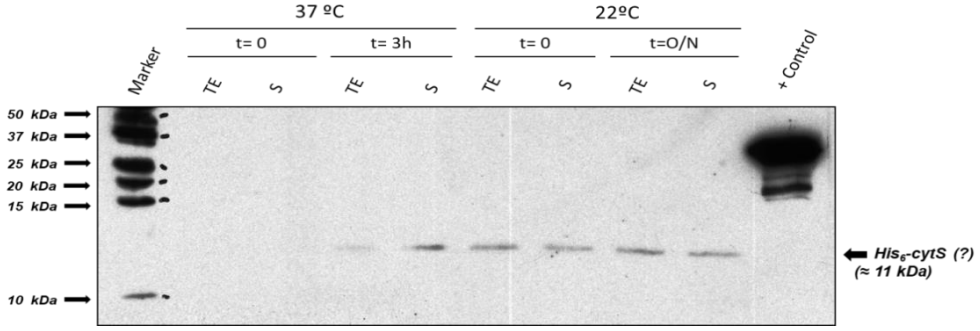

Figure 4.7 - Western Blot visualization of His-tagged cytS expression tests in *E. coli* BL21(DE3) samples. The same lysates used in BL21(DE3) expression tests samples shown in Figure 4.6 as well as a known His-tagged protein sample as a positive control were loaded on a 17% SDS-PAGE, transferred to a nitrocellulose membrane and then incubated with mouse-**α-**His primary antibody followed by goat-**α-**mouse horseradish peroxidase labelled secondary antibody. Visualization by the ECL method with an exposure of 3 minutes. Expected position of cytS on the right.

While the SDS-PAGE gel of the expression tests using two strains at different temperatures and times of induction does not show a distinctive 11 kDa induced protein band, the Western blot analysis of the BL21(DE3) samples of both sets of conditions (3 hours at 37ºC or ON at 22ºC) reveals a faint band around the expected molecular weight (11 kDa). Still, the level of expression is clearly too low for biochemistry studies. Ultimately, as it was not possible to obtain a reasonable expression level for KhtS (full-length or cytosolic-segment) in any of the conditions tested the endeavor of expressing and studying KhtS at a biochemical level was abandoned from this point forward.

4.1.3. KhtU Expression Vector Testing

Regarding the *khtSTU* operon membrane protein KhtU, three different constructs were built in order to test which expression system was the best: pRSFDuet:*khtU* (membrane protein alone, N-terminally His_6-tagged); pRSFDuet:*khtU*+*khtT* (membrane protein N-terminally His_6-tagged in MCS1 and the ancillary protein in MCS2, untagged) and pET24dT:*khtTU* (partial operon segment, starting in KhtT and ending in KhtU, C-terminally His_6-tagged). Each construct was tested as described in section 3.3.

Figure 4.8 represents the result of the small-scale expression and crude purification tests for the three KhtU-related constructs. KhtU was identified by Western Blotting using an αHis antibody. In addition, since KhtU is the only His-tagged protein the eventual presence of KhtT on the elution fraction would mean that it was previously bound to KhtU, suggesting a complex-like binding.

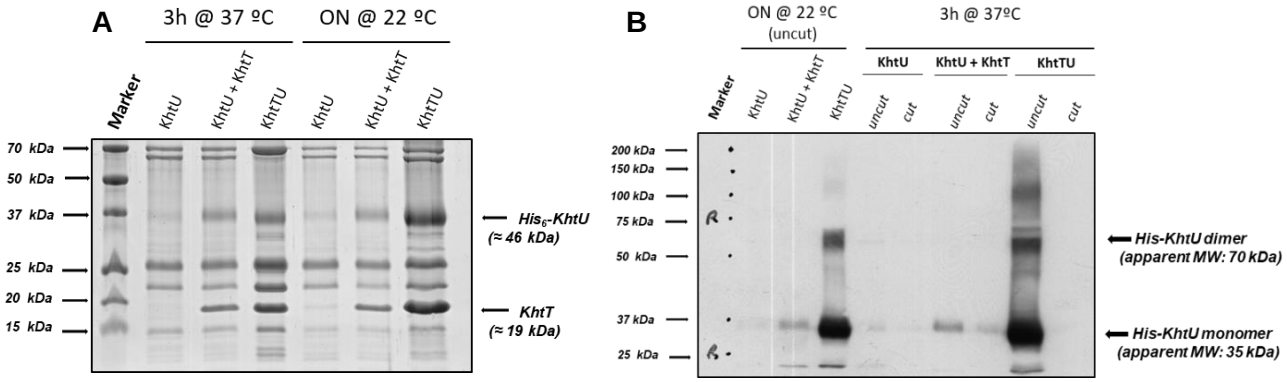

Figure 4.8 - SDS-PAGE gel and Western Blot of the small-scale purification test results for KhtU expression vectors (KhtU; KhtU+KhtT and KhtTU). Each vector was induced in two different conditions (3 hours at 37 ºC or overnight at 22 ºC). A small-scale detergent extraction and purification protocol performed for each condition using IMAC with nickel beads yielded a protein fraction containing His_6-tagged KhtU (and contaminants). **(A)** 15% SDS-PAGE gel analysis of the fractions obtained in each test, as the legend above describes. **(B)** Western Blot visualization of a 10% SDS-PAGE gel of His-tagged and thrombin-digested (tagless) test samples of each construct using a mouse-α-His primary antibody and a horseradish peroxidase labeled goat-α-mouse secondary antibody to determine which band corresponds to KhtU. Exposure of 1 second. Ponceau staining of the membrane in Appendix. Markers used: Bio-Rad's Precision Plus Protein™ All Blue Prestained Protein Standards.

Membrane proteins can display a different migration behavior in SDS-PAGE from what is expected for their actual molecular weight. This seems to be the case with KhtU, since the western blot showed that the protein monomer is running at an apparent molecular weight of approximately 35 kDa, despite its predicted molecular weight being 46 kDa. As seen on **Figure 4.8**, all three constructs exhibit expression of KhtU. However, in the case of pRSFDuet:*khtU*, the vector with the membrane protein expressed alone, the expression level is much lower than for the other two vectors, pRSFDuet:*khtU*+*khtT* and pET24dT:*khtTU*. KhtT appears on the elution fraction of both KhtU+KhtT and KhtTU samples, suggesting that KhtT forms a complex with KhtU; this happens regardless of them being coded in separate promoters or in an operon-like manner.

Based on its higher expression level the operon-like KhtTU vector was selected for further experiments.

4.1.4. KhtTU Expression and Purification

Following small-scale expression tests for KhtTU and selection of the most appropriate expression vector, large-scale purification of the KhtTU construct was attempted and optimized. The protocol for KhtTU purification consists on the following steps: cell lysis, membrane protein extraction and solubilization by DDM (a non-ionic detergent) followed by IMAC purification using nickel beads, His-tag digestion and size-exclusion chromatography. Samples of each step of the extraction and purification protocol were analyzed by SDS-PAGE (**Figure 4.9**).

The elution profile from the size-exclusion chromatography (**Figure 4.10** A) shows a main peak around 12 mL (corresponding to the KhtTU complex), as well as two other smaller peaks around 15 mL and 17 mL (corresponding to uncomplexed KhtT and undisclosed contaminants, respectively), confirmed by SDS-PAGE analysis of each peak fraction (**Figure 4.10** B).

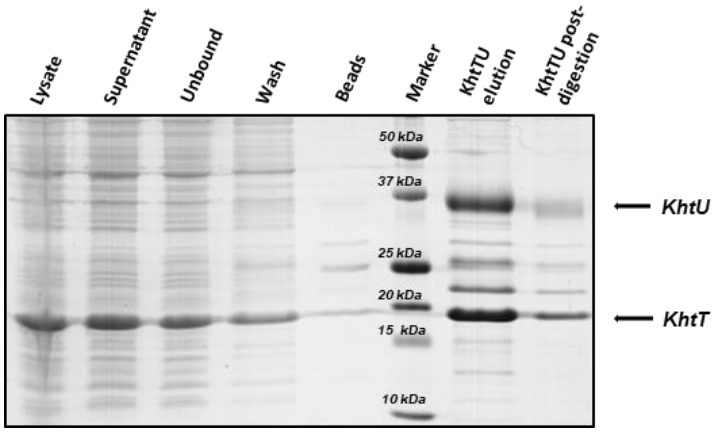

Figure 4.9 - SDS-PAGE gel of KhtTU complex extraction and IMAC purification steps. Cell lysate was incubated overnight with 20 mM DDM and 5% glycerol at 4 ºC for membrane protein extraction. Following IMAC purification step, KhtTU complex was eluted using 150 mM Imidazole in the Elution Buffer. Incubation with thrombin during overnight dialysis yielded tagless KhtU. Each sample was loaded in the gel as the legend above describes. Markers used: Bio-Rad's Precision Plus Protein™ All Blue Prestained Protein Standards. The relatively high percentage of contamination is due to low levels of membrane protein expression and low specificity of the nickel beads.

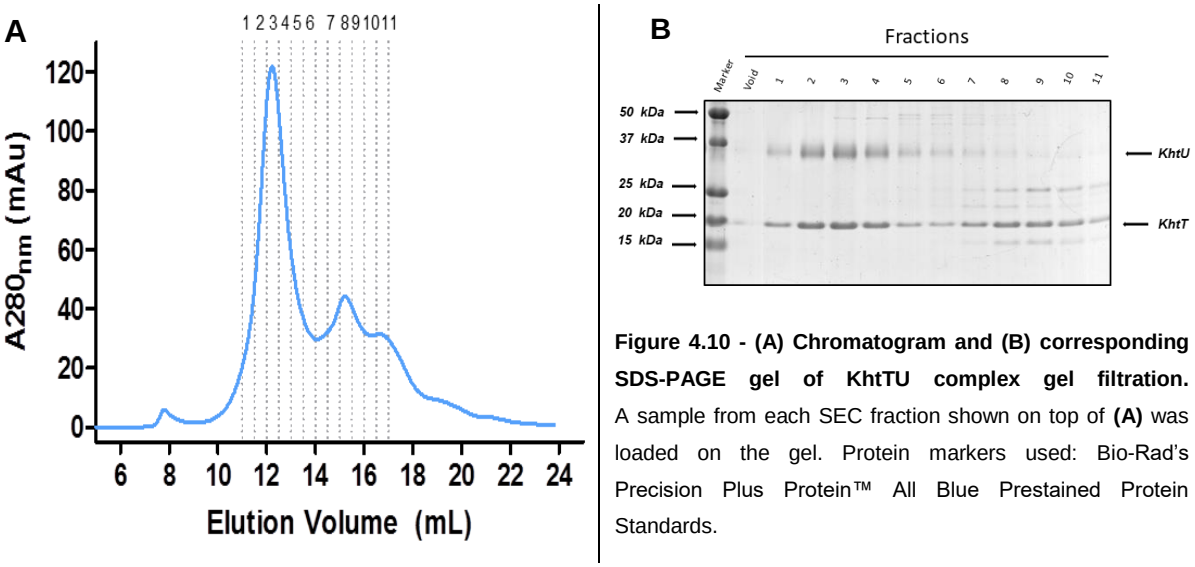

Figure 4.10 - (A) Chromatogram and (B) corresponding SDS-PAGE gel of KhtTU complex gel filtration. A sample from each SEC fraction shown on top of **(A)** was loaded on the gel. Protein markers used: Bio-Rad's Precision Plus Protein™ All Blue Prestained Protein Standards.

In order to test the stability of the KhtTU complex over time, the protein complex fraction resulting from size-exclusion chromatography was concentrated and re-injected into the same column after being left overnight at 4 ºC. The result of this test is shown in **Figure 4.11**. The profile shows that the complex is relatively stable overtime, since only 20% of the complex sample injected dissociated (comparing peak absorbances).

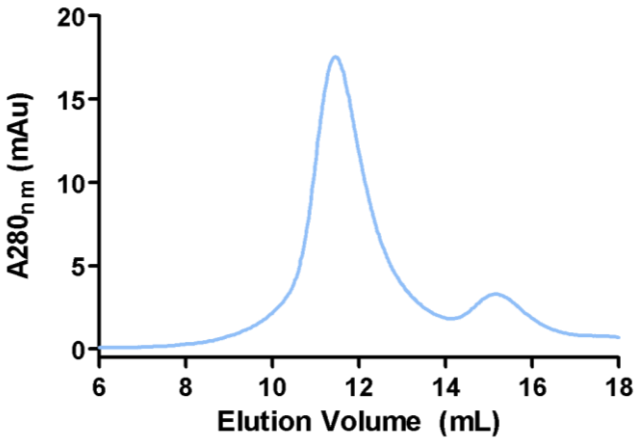

Figure 4.11 - Chromatogram of the overnight stability test for the KhtTU complex.

A pure sample of KhtTU complex resulting from the purification step shown in Figure 4.10 was reinjected in the column after being left at 4ºC overnight as a stability test. The first peak corresponds to the KhtTU complex and the second to KhtT alone.

The expression and purification protocol developed yields approximately 150 µg of pure KhtTU complex per liter of culture, a relatively high quantity in terms of membrane protein expression. Accordingly, the protocol for large-scale purification of KhtTU complex shown in this work was deemed appropriate for further biochemical and crystallographic experiments.

4.1.5. Expression of the Selenomethionine Variant of KhtT

In the process of obtaining a crystallographic structure for KhtT it was necessary to generate a selenomethionine variant of this protein to overcome the phase problem. As such, a modified expression protocol had to be performed. Production of SeMet-KhtT was achieved using a methionine auxotroph strain of *E. coli* and minimal media lacking L-Methionine but supplemented with L-Selenomethionine. Otherwise, both expression and purification methodologies applied were the same as those of native KhtT. The result of the extraction and IMAC purification steps is shown in **Figure 4.12**. The size exclusion chromatography profile of this variant shows no discernible difference in either peak volume or shape and as such is not illustrated in this chapter. SeMet variant of KhtT was concentrated after purification and used in crystallization trials.

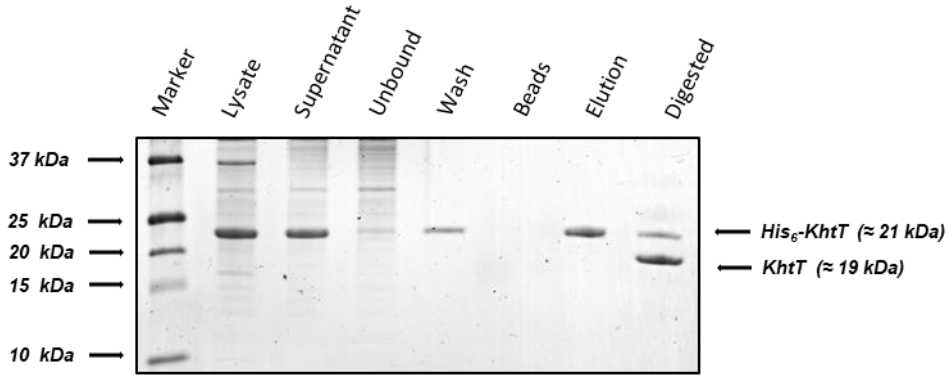

Figure 4.12 - SDS-PAGE of the extraction and IMAC purification steps of the selenomethionine variant of KhtT (SeMet KhtT). Protein was obtained after loading a spin-cleared cell extract supernatant in a nickel affinity column, washing it and eluting the protein with 50 mM Imidazole, exactly like native KhtT. Each sample was loaded on the gel as the legend above it describes. Protein markers used: Bio-Rad's Precision Plus Protein™ All Blue Prestained Protein Standards. Arrows to the right mark the expected position of the protein.

4.2. Ligand Testing by Thermal Shift Assay

It has been thought that KhtT has a regulatory role but no KhtT ligands have been described in the literature. As such, for both structural and functional studies an attempt was made to discover a ligand for this protein. The first technique used for this goal was differential scanning fluorimetry (DSF), also known as Thermal Shift Assay. The theoretical basis for this technique lies on changes of the thermal stability of a given protein due to changes in pH, ionic strength, or presence of additives, mutations or even ligands. In DSF, an external fluorescent dye (SYPRO Orange) is used for its ability to bind to hydrophobic regions of a protein. The protein is unfolded as the result of an increase in temperature, exposing hydrophobic regions to the solvent, allowing the dye to bind and increase its fluorescence signal. Further increases in temperature lead to protein aggregation and fluorescence quenching. As such, there is a clear fluorescence transition due to temperature induced protein unfolding. The melting temperature is defined as the mid-point of such transition, which can easily be determined by calculating the 1^{st} derivative of experimental curve. The thermal stability of a protein is directly related to its melting temperature (Tm) and a positive shift of this parameter is usually an indication that the molecule being tested stabilizes the protein and, as such, is a potential ligand. Comparing melting temperatures of untreated and ligand supplemented samples usually yields a ΔTm, which indicates thermal stabilization or destabilization, and different ligands can be compared using this value [64].

The first step in ligand screening was the determination of the melting temperature for KhtT in the buffer used for its purification, without any ligand being added. After establishing this value, several ligands were added at high concentrations (to force the bound state) in parallel samples. At first, random screening of biological ligands was tested (nucleotides, amino acids, metal ions, redox-related coenzymes) without success. Then, other potential ligands identified from existing literature were tested: cyclic dinucleotides (**Figure 4.13**) and bacillithiol (**Figure 4.14**).

KhtT's melting temperature in its purification buffer was defined as 70.8 ± 1.5 ºC (n = 27). This value was then compared with the melting temperature of the protein in the presence of the different ligands tested (**Table 4.1**).

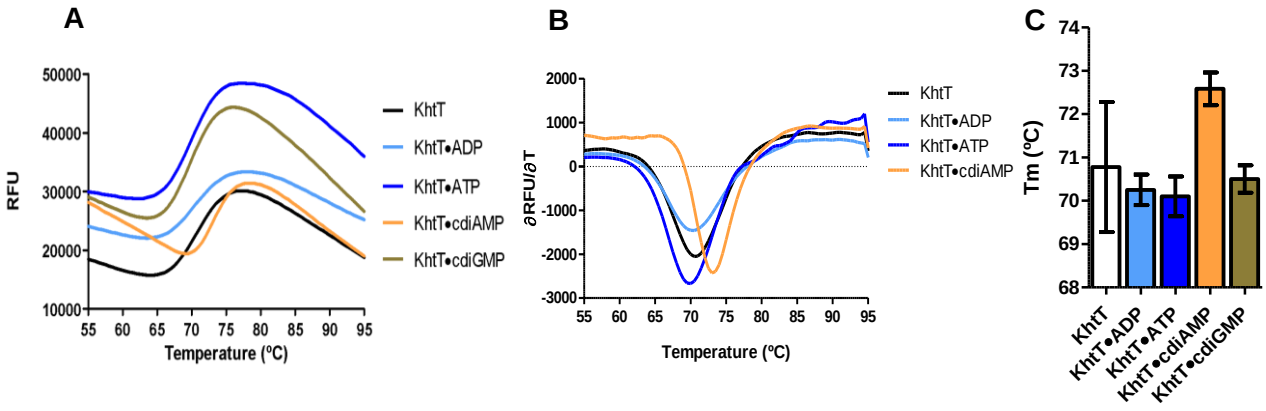

Figure 4.13 - Thermal shift assay ligand testing results for KhtT supplemented with nucleotide ligands. Representative **(A)** Melting curves, **(B)** corresponding 1st derivative curves and **(C)** bar graph data treatment of KhtT control and ligand testing samples of some of the nucleotides tested in the assay: ADP, ATP; c-di-AMP and c-di-GMP. Error bars correspond to standard deviation of n=27 for the control, n=10 for the ADP and ATP samples and n=6 for the c-di-AMP and c-di-GMP samples.

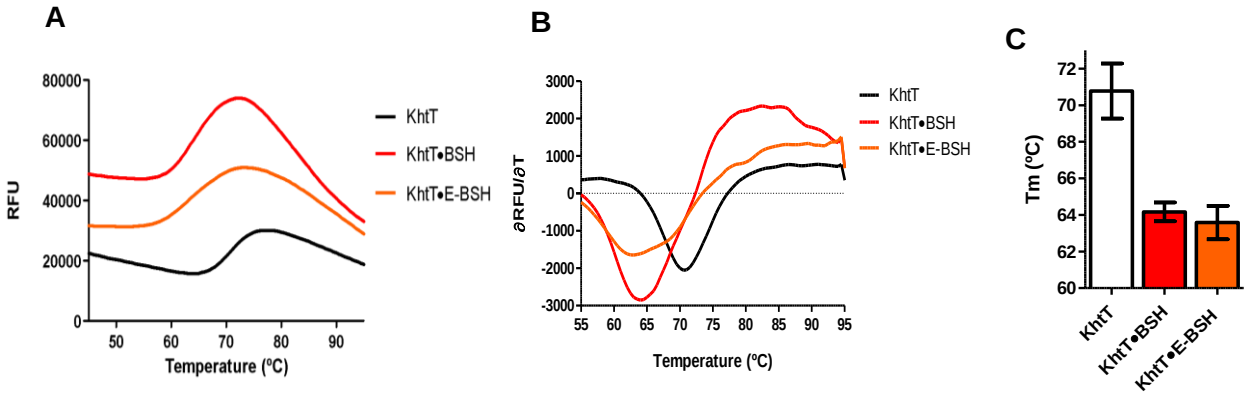

Figure 4.14 - Thermal shift assay ligand testing results for KhtT supplemented with bacillithiol. Representative **(A)** Melting curves, **(B)** corresponding 1st derivative curves and **(C)** bar graph data treatment of KhtT control and ligand testing bacillithiol samples in both oxidized (BSH) and reduced (ethylmaleimide-bacillithiol, E-BSH) states. Error bars correspond to standard deviation from n=27 for the control and n=6 for the BSH and E-BSH samples.

Table 4.1 - Melting temperature [(Tm (ºC)] values obtained for KhtT in the presence of different ligands.
Legend: Number of repetitions (n), standard deviation (SD) and Tm shift for each ligand used.

Ligand	n	Tm (ºC)	SD	ΔTm
KhtT control	27	70.8	1.50	-
ATP	10	70.1	0.46	- 0.7
ADP	10	70.3	0.35	- 0.5
c-di-AMP	6	72.6	0.38	+ 1.8
c-di-GMP	6	70.5	0.32	- 0.3
BSH	6	64.2	0.52	- 6.6
E-BSH	6	63.6	0.92	- 7.2

Of the tested adenosine-nucleotides and cyclic dinucleotides, common ligands of regulatory subunits of potassium transporters in *Bacillus subtilis*, only c-di-AMP showed a positive ΔTm (≈ 2 ºC); 2 ºC is the minimal temperature shift indicating a relevant result. The effect caused by c-di-AMP appears to be specific, since c-di-GMP has no effect (**Figure 4.13** C and **Table 4.1**). Thus, c-di-AMP was selected as a potential ligand and chosen for further testing.

Previous studies have suggested that bacillithiol, an antioxidant thiol produced in Bacilli, could be a ligand of the KhtTU antiporter. Binding of bacillithiol was proposed to be related to detoxification and oxidative stress resistance mechanisms, as discussed in section 1.4. Therefore, bacillithiol (in both oxidized and reduced states) was also tested in these ligand testing assays. However, there are some problems with the way these compounds were prepared: BSH_2 in salt form was ordered from Vanderbilt University. Reduced BSH was generated by incubation with 2 mM TCEP but the resulting product was not evaluated. Furthermore, alkylation of BSH by N-ethylmaleimide (rendering E-BSH) was performed in the laboratory without assessing the product. In any case, the melting temperature of KhtT decreased by approximately 7ºC upon addition of these compounds (**Figure 4.14** C and **Table 4.1**), which means that the protein became less stable in their presence. This suggests that bacillithiol is not a ligand of KhtT, although it could be a ligand of the KhtTU complex.

Other molecules may bind to KhtT and perform a physiological role as ligands. However, no further screening was done to focus on confirmation and characterization of c-di-AMP's binding to KhtT using other techniques.

4.3. Isothermal Titration Calorimetry Assays

Isothermal Titration Calorimetry (ITC) was used to further characterize the binding properties of c-di-AMP binding to KhtT. In this technique small amounts of ligand are injected into a cell containing protein and heat changes (release or absorption) resulting from the ligand-protein interaction are detected. As the ligand saturates its binding sites the amount of heat measured per injection decreases allowing for the determination of binding enthalpy (ΔH), the association constant K_A and the stoichiometry of the reaction *n*. From these values, other parameters of the binding reaction can be calculated, such as Gibbs free energy (ΔG) and the entropy factor (-TΔS). [65]

The first set of experiments consisted on the titration of c-di-AMP into a cell containing pure KhtT, as well as its reverse titration, as described in section 3.8. Representative curves of both types of injection are shown in **Figure 4.15**. AFFINImeter software was used to simultaneously fit the data from 5 different titrations (3 forward and 2 reverse) using a single binding site model (such as A+B → AB) (fit results on **Table 4.2** and **Figure 4.16**). Heat of dilution of c-di-AMP titrated into buffer was subtracted from ligand titration data (Appendix, **Figure 8.2**).

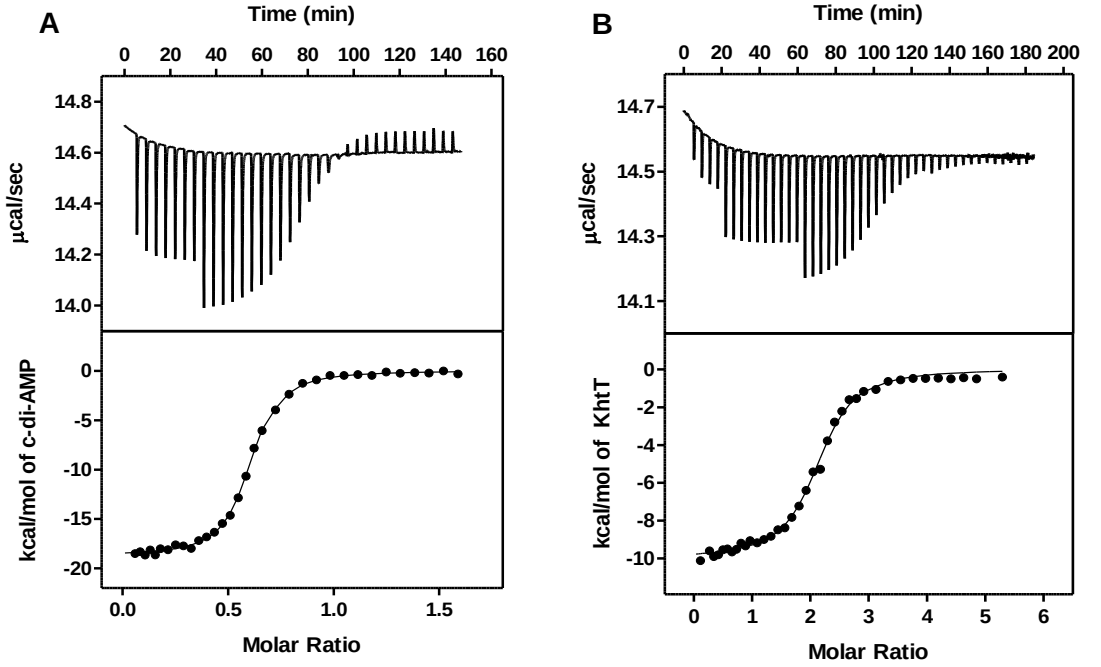

Figure 4.15 - Representative ITC curves of interaction studies of c-di-AMP and KhtT. **(A)** Forward titration: 20 µM of pure KhtT titrated with 150 µM c-di-AMP; **(B)** Reverse titration: 6 µM of c-di-AMP titrated with 175 µM KhtT. The top panels show the raw titration heat values (µcal/sec) plotted against time. The bottom panels show normalized integration heat values (kcal/mol) of injectant plotted against molar ratio. Temperature used: 25 ºC.

Table 4.2 - Thermodynamic parameters determined for the binding interaction between KhtT (monomer) and c-di-AMP, calculated by a global analysis of 5 different runs.

n (sites) =	0.547 ± 0.0005 (1:2)
K_A (M^{-1}) =	7.24 x10^6 ± 0.07 x10^6 *
K_D (M) =	1.38 x10^{-7} ± 0.01 x10^{-7} *
ΔH (kcal/mol) =	-22.84 ± 0.014
ΔG (kcal/mol) =	-9.36
-TΔS (kcal/mol) =	13.48

**Statistical error of the fit*

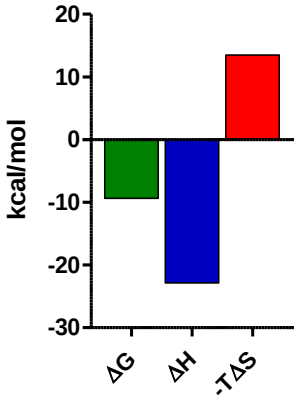

Figure 4.16 - Binding signature (Gibbs Free Energy ΔG, binding enthalpy ΔH and entropy factor –TΔS) obtained for the binding reaction of KhtT with c-di-AMP.

The ITC results displayed above show an exothermic binding reaction occurring between KhtT and c-di-AMP. The enthalpy of the reaction was determined as -22.84 kcal/mol, with a dissociation constant of 1.38 $x10^{-7}$ M (138 nM) and a stoichiometry of interaction (n) of approximately 0.5, meaning that 1 molecule of c-di-AMP is bound to 2 molecules of KhtT. Note that it was determined above that KhtT in solution is likely to be a dimer. The binding signature, showing a negative binding enthalpy and a positive entropic factor suggests that the interaction between c-di-AMP and KhtT is enthalpy-driven and dominated by the formation of new polar interactions with the ligand and possibly within the KhtT dimer. In addition, the large entropy decrease could indicate an increase in the ordering of the protein dimer upon ligand binding.

ITC experiments were also performed with c-di-GMP. Representative curves of the titrations are shown in **Figure 4.17**.

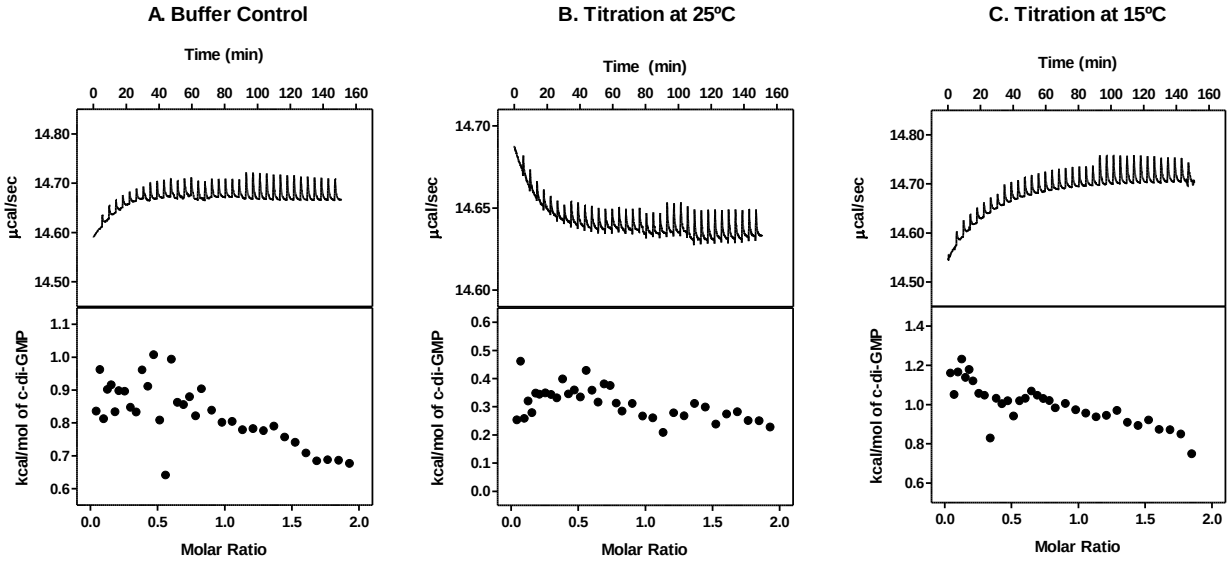

Figure 4.17 - Representative ITC curves of interaction studies for KhtT and c-di-GMP. (A) Injection of 300 µM c-di-GMP into buffer, as a control; **(B)** 35 µM of pure KhtT titrated with 300 µM c-di-GMP at 25ºC; **(C)** 35 µM KhtT titrated with 300 µM c-di-GMP at 15ºC; The top panels show the raw titration heat values (µcal/sec) plotted against time. The bottom panels show their respective normalized integration heat values (kcal/mol) of injectant plotted against molar ratio.

C-di-GMP titrations were performed at two different temperatures and the heat exchanged by injecting the ligand to the protein is similar to heat of dilution measured from the buffer control in both. This strongly indicates that c-di-GMP does not bind to KhtT, demonstrating that the interaction with c-di-AMP is specific. Overall, these ITC results are consistent with the results shown in the Thermal Shift Assay section.

4.4. Controlled Proteolysis Assay

The effect of c-di-AMP in KhtT's structural conformation was studied by a controlled proteolysis assay, which consists in incubating different protease-to-protein ratios for a fixed amount of time in the presence and absence of the ligand in question and observing the digestion pattern by SDS-PAGE visualization. An eventual change in the structure of the protein when bound to the ligand may make it less prone to proteolysis, which in turn suggests the ligand stabilizes the protein structure.

In this experiment, small quantities of trypsin and chymotrypsin were used to test whether c-di-AMP enhances KhtT's proteolytic resistance. The digestion patterns displayed in **Figure 4.18** show that samples previously incubated with this ligand are more resistant to proteolysis by these two enzymes, since most of the protein remains at higher molecular weight segments while untreated samples were digested faster and to a higher extension. These results together with those obtained with Thermal Shift Assay and Isothermal Titration Calorimetry further demonstrate that c-di-AMP acts as a ligand of KhtT and causes a structural change.

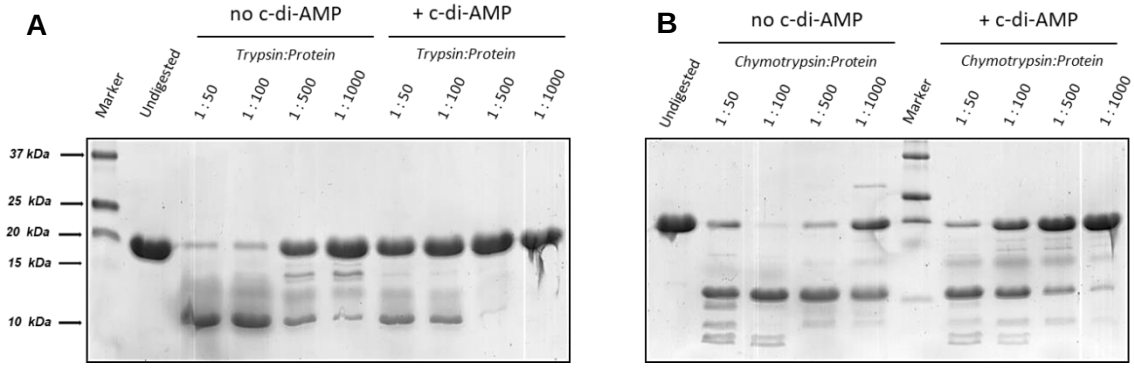

Figure 4.18 - SDS-PAGE gels of KhtT controlled proteolysis assays in the presence and absence of c-di-AMP. 15 µg of protein (50 µM) used per sample. Different protease-to-protein ratios (ratios shown above, using either **(A)** trypsin or **(B)** chymotrypsin) were incubated with and without 50 µM c-di-AMP for 1 hour at room temperature. Reaction was stopped with the addition of SDS-PAGE sample buffer and each sample was loaded in a 17% gel. Protein markers used: Bio-Rad's Precision Plus Protein™ All Blue Prestained Protein Standards.

4.5. KhtTU Antiporter Activity Assay

At this point, it is clear that c-di-AMP binds to KhtT with high affinity (K_D ~100 nM) and induces a structural change in the protein. However, none of the assays performed correlate c-di-AMP binding with the function of KhtTU. As such, a functional assay consisting on measuring the antiporter activity of KhtTU in everted vesicles was setup, based on the method described by Rosen [66], consisting on the following steps: overexpression of KhtTU in KNabc cells (an antiporter-deficient *E. coli* strain) followed by the preparation of everted vesicles by French Press. These vesicles contain the membrane proteins of the cell in a reversed orientation (the lumen of the vesicle corresponds to the extracellular space while the outside of the vesicle corresponds to the intracellular space). At this stage, a membrane-binding fluorophore (ACMA) is added to the vesicles. This fluorophore quenches in the presence of a proton gradient (ΔpH) across the membrane. At the beginning of the assay, ACMA's signal is detected since no ion gradient exists (**Figure 4.19 A**). The addition of D-lactate to the vesicles energizes the respiratory chain, which pumps protons to the lumen creating a proton gradient and ACMA fluorescence is quenched (**Figure 4.19 B**). At this point, the activity of KhtTU can be studied by generating a cation (e.g. KCl) gradient outside the vesicles. Given the antiporter activity of KhtTU, cation and protons are exchanged, dissipating the proton gradient, which in turn leads to the dequenching of ACMA fluorescence (**Figure 4.19 C**). The rate of dequenching can be related to antiporter activity.

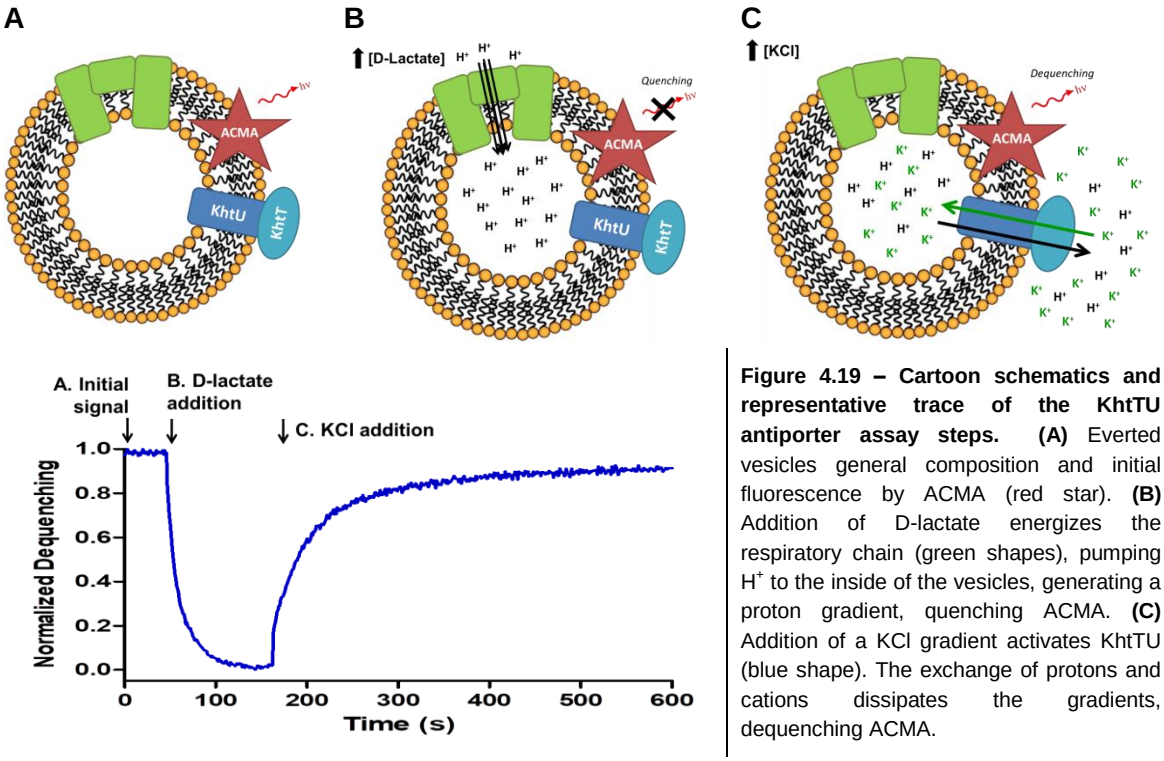

Figure 4.19 – Cartoon schematics and representative trace of the KhtTU antiporter assay steps. **(A)** Everted vesicles general composition and initial fluorescence by ACMA (red star). **(B)** Addition of D-lactate energizes the respiratory chain (green shapes), pumping H^+ to the inside of the vesicles, generating a proton gradient, quenching ACMA. **(C)** Addition of a KCl gradient activates KhtTU (blue shape). The exchange of protons and cations dissipates the gradients, dequenching ACMA.

The assay shows a basal activity when vesicles have KhtTU and no cation is added (**Figure 4.20**). However, generation of a K^+ gradient directed inward by addition of KCl gives rise to an increase in proton flux that is consistent with the H^+/K^+ antiport activity proposed for the KhtTU protein complex. The basal activity observed in the absence of added K^+ could result either from proton leak as uniport through KhtTU or from antiport because of contaminant K^+ in the experimental system. Experiments in the absence and in the presence of 10 μM of c-di-AMP clearly show that c-di-AMP activates proton flux.

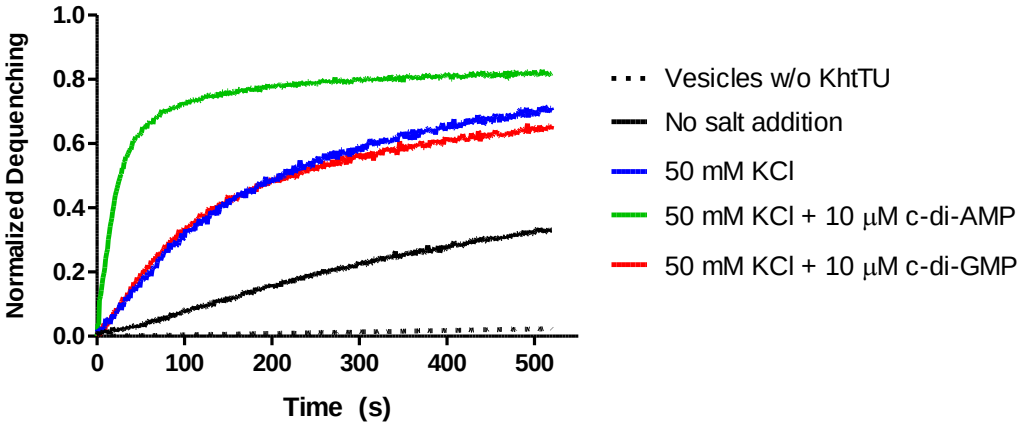

Figure 4.20 - Comparison of K^+/H^+ antiporter activity of KhtTU in the presence of c-di-AMP and c-di-GMP against basal activity in everted vesicles. Example curves of the time dependent change of ACMA fluorescence when 50 mM KCl was added to the sample at pH 8.5 after a steady-state ΔpH was obtained by addition of 4 mM lactate. **Legend: Dots –** Vesicles without KhtTU (negative control); **Black –** No addition of any salt; **Blue –** Addition of 50 mM KCl; **Green –** Addition of 10 μM c-di-AMP followed by 50 mM KCl; **Red –** Addition of 10 μM c-di-GMP followed by 50 mM KCl. All curves obtained in triplicates at room temperature.

Fitting of the curves was made using GraphPad Prism, a curve fitting and scientific graphing software. First, a one-phase exponential fit was attempted. However, some of the curves did not fit using this equation alone, so other models were tried. Ultimately, a 2-phase exponential equation was deemed appropriate to fit the data that could not be fitted with a single exponential (**Figure 4.21**). This equation presents two rate constants (k_{fast} and k_{slow}): k_{slow} was interpreted as the rate of background dequenching as it is very similar to the rate of basal activity observed without the addition of KCl and is insensitive to the addition of ligand while k_{fast} was interpreted as the rate constant corresponding to KhtTU activity and it responds to changes in the concentration of c-di-AMP.

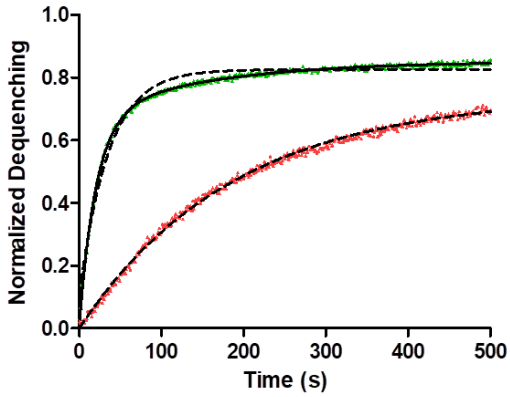

1-phase exponential fit equation:

$$\%\boldsymbol{Dequenching} = \boldsymbol{A}(\mathbf{1} - \boldsymbol{e}^{-\boldsymbol{kt}})$$

$$(A = Max_{Dequenching} - Min_{Dequenching})$$

2-phase exponential fit equation:

$$\%\boldsymbol{Dequenching} = \boldsymbol{A_{fast}}\left(\mathbf{1} - \boldsymbol{e}^{-\boldsymbol{k_{fast}t}}\right) + \boldsymbol{A_{slow}}(\mathbf{1} - \boldsymbol{e}^{-\boldsymbol{k_{slow}t}})$$

$$(A_{fast} = (Max - Min) * \%_{fast} * 0.01)$$

$$(A_{slow} = (Max - Min) * \%_{slow} * 0.01)$$

Figure 4.21 – Fitting process of the antiporter assay curves. A single exponential equation was attempted first, but this only correctly fit some of the curves (dotted line over both curves). Other curves could only be fitted using a two-phase exponential (full line over the green curve).

The same process was then applied to every sample performed in this assay. A comprehensive table of the kinetic parameters determined for every sample in presented below.

Table 4.3 – Kinetic parameters determined by 1- or 2-phase exponential fitting of the KhtTU antiporter assay curves. Description of each sample followed by the rate constants and the standard deviation (SD) of n=3 samples.

	KhtTU Antiporter Assay Fit Parameters									
	1-phase		2-phase							
Sample Description	**k (s^{-1})**	**SD**	**%fast**	**SD**	**%slow**	**SD**	**k_{fast} (s^{-1})**	**SD**	**k_{slow} (s^{-1})**	**SD**
Vesicles without KhtTU	0.00	0.00								
No salt addition	1.45E-03	0.18E-03								
pH 8.5 :										
50 mM KCl	5.30E-03	0.07E-03								
50 mM KCl + 50 nM c-di-AMP	6.33E-03	0.09E-03								
50 mM KCl + 200 nM c-di-AMP	7.79E-03	0.07E-03								
50 mM KCl + 500 nM c-di-AMP	7.00E-03	0.14E-03								
50 mM KCl + 1 µM c-di-AMP			58.41	18.96	41.59	18.96	12.1E-03	2.91E-03	3.13E-03	2.52E-03
50 mM KCl + 2 µM c-di-AMP			67.40	2.41	32.60	2.41	28.8E-03	1.23E-03	6.34E-03	0.53E-03
50 mM KCl + 5 µM c-di-AMP			61.94	1.36	38.06	1.36	45.1E-03	1.69E-03	7.62E-03	0.35E-03
50 mM KCl + 10 µM c-di-AMP			78.36	1.88	21.64	1.88	48.2E-03	2.44E-03	6.71E-03	0.93E-03
50 mM KCl + 10 µM c-di-GMP	6.74E-03	0.14E-03								
50 mM KCl + 50 µM BSH	6.65E-03	0.08E-03								
50 mM KCl + 50 µM E-BSH	7.52E-03	0.10E-03								
50 µM BSH control	1.25E-03	0.03E-03								
50 µM E-BSH control	5.39E-03	0.04E-03								
200 mM NaCl	6.33E-03	0.05E-03								
200 mM NaCl + 10 µM c-di-AMP	6.88E-03	0.10E-03								
50 mM RbCl	6.79E-03	0.12E-03								
50 mM RbCl + 10 µM c-di-AMP			75.25	0.53	24.75	0.53	119.6E-03	2.97E-03	9.34E-03	0.32E-03

The experiments displayed in **Figure 4.20** clearly show that c-di-AMP increases the flux of protons. The apparent rate constant of flux (**Table 4.3**) determined for KhtTU in the presence of 10 μM c-di-AMP (k_{fast} = 48.2 ± 2.44 x10^{-3} s^{-1}) is 9 times higher than in its absence (k = 5.30 ± 0.07 x10^{-3} s^{-1}). Furthermore, c-di-GMP does not cause a significant change on the flux (k = 6.74 ± 0.14 x10^{-3} s^{-1}, only 1.3 times higher than the basal rate).

In order to further characterize the functional impact of c-di-AMP on KhtTU, a titration using concentrations of ligand spanning from 50 nM to 10 μM was performed and a dose-response curve was plotted (**Figure 4.22** and **Figure 4.23**). The EC_{50} for the binding was estimated as 1.97 ± 0.07 μM of c-di-AMP. This value is very different from the c-di-AMP constant of dissociation for binding (K_D = 138 nM) previously measured for KhtT alone but is still within the range of physiological concentrations of c-di-AMP found in B. subtilis (2 to 5 μM).

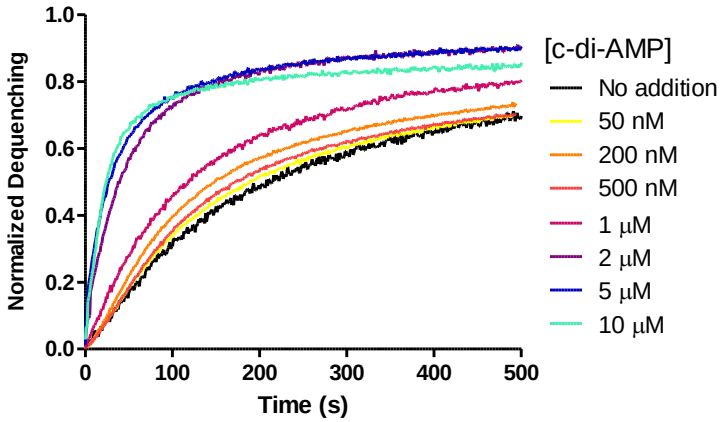

Figure 4.22 - Kinetic curves for the titration of KhtTU vesicles with c-di-AMP. Normalized kinetic curves of changes in ACMA fluorescence when 50 mM KCl and different concentrations of c-di-AMP were added to the sample at pH 8.5. Fitting of each curve using a one-phase or two-phase association non-linear regression. All curves obtained in triplicates at room temperature.

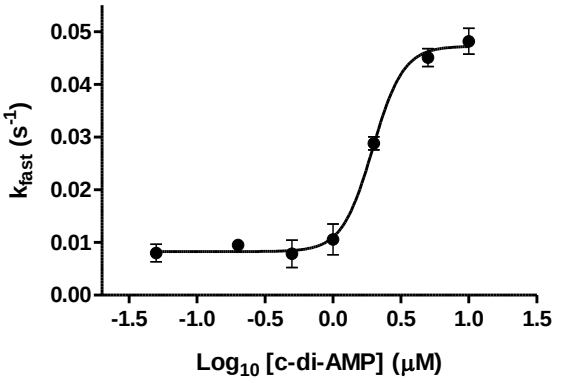

$$k_{fast} = Min + \frac{Max - Min}{1 + 10^{(LogEC50 - Log[c-di-AMP]) * Slope}}$$

Figure 4.23 - Dose-response curve of the titration of KhtTU vesicles with c-di-AMP.
The k_{fast} values obtained from the fitting of each curve shown in Figure 4.22 were plotted against the Log_{10} of ligand concentration. The EC_{50} obtained for the binding was determined as 1.97 ± 0.07 μM of c-di-AMP, using the equation shown below the graph.

Following this experiment, another question was made: Is KhtTU able to transport other monovalent cations besides potassium and, if so, does c-di-AMP affect their transport as well? The question was answered by creating gradients of different monovalent cation salts both in the presence or absence of 10 μM c-di-AMP (**Figure 4.24**).

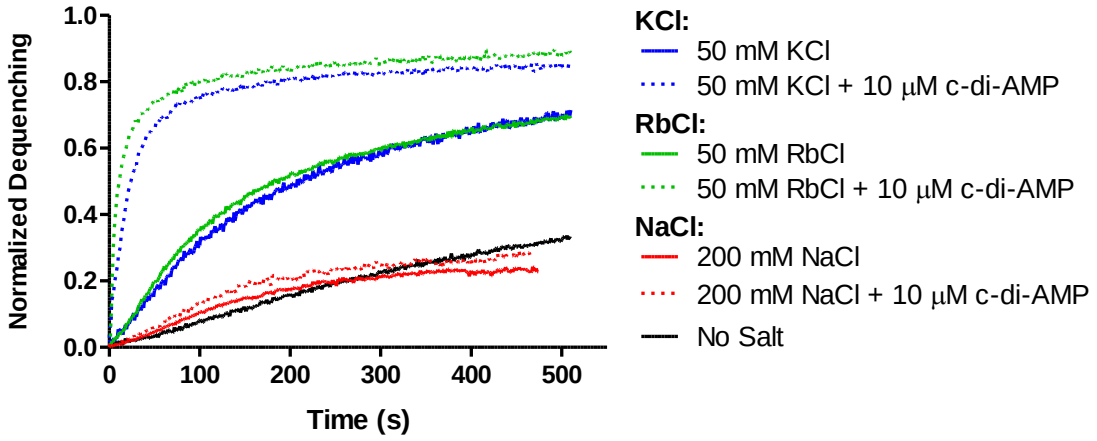

Figure 4.24 - Cation/Proton antiport activity of everted vesicles containing KhtTU in different monovalent cation gradients with and without 10 μM c-di-AMP. Example curves of the time dependent change of ACMA fluorescence when 50 mM KCl, 50 mM RbCl or 200 mM NaCl were added to the sample at pH 8.5 after a steady-state ΔpH was obtained by addition of 4 mM lactate. **Legend: Black –** No addition of any salt; **Red line -** Addition of 200 mM NaCl; **Red dots -** Addition of 10 μM c-di-AMP followed by 200 mM NaCl; **Green line –** Addition of 50 mM RbCl; **Green dots –** Addition of 10 μM c-di-AMP followed by 50 mM RbCl; **Blue line –** Addition of 50 mM KCl; **Blue dots –** Addition of 10 μM c-di-AMP followed by 50 mM KCl. Fitting of each curve using a one-phase or two-phase association non-linear regression. All curves obtained in triplicates at room temperature.

According to the results shown in **Figure 4.24** and **Table 4.3**, KhtTU antiport occurs with rubidium (Rb^+) as well as with potassium (K^+) and the effect of c-di-AMP on the rate of proton transport is approximately the same regardless of which of these two cations is being transported. In contrast, proton antiport is not stimulated by addition of sodium (Na^+), and c-di-AMP does not enhance the activity of KhtTU when this cation was tried. Overall, this suggests that KhtTU is selective for potassium and larger monovalent cations relative to sodium and the effect of c-di-AMP is independent of the cation being transported.

The last set of experiments performed with this assay was once again to test the hypothesis postulated by Helmann and colleagues [42] that suggested that KhtTU is regulated by bacillithiol and its adducts.

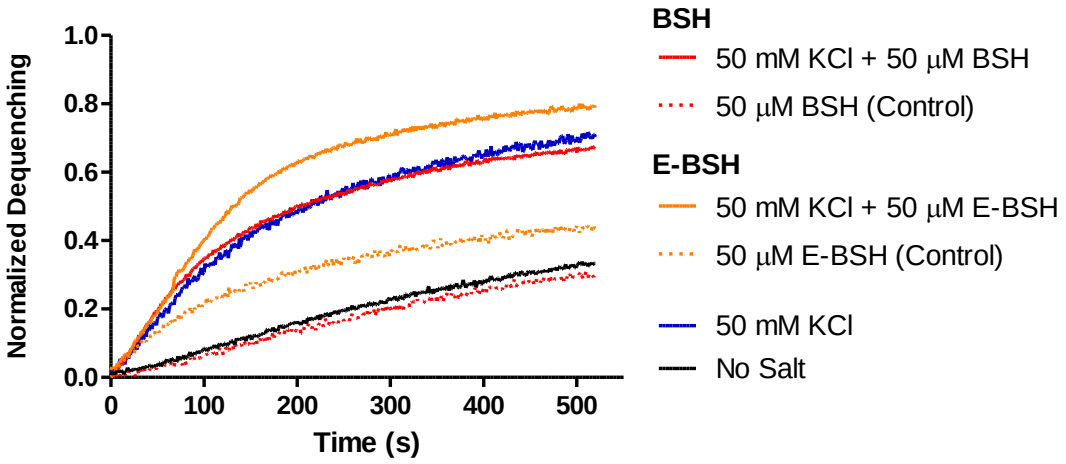

Figure 4.25 - Comparison of K^+/H^+ antiporter activity of everted vesicles containing KhtTU in the presence of reduced bacillithiol (BSH) and its oxidized form ethylmaleimide-bacillithiol (E-BSH) against basal activity. Example curves of the time dependent change of ACMA fluorescence when 50 mM KCl was added to the sample at pH 8.5 after a steady-state ΔpH was obtained by addition of 4 mM lactate. **Legend: Black line –** No addition of any salt; **Blue line –** Addition of 50 mM KCl; **Orange dots -** Addition of 50 μM E-BSH alone; **Orange line –** Addition of 50 μM E-BSH followed by 50 mM KCl; **Red dots –** Addition of 50 μM BSH alone; **Red line –** Addition of 50 μM BSH followed by 50 mM KCl. Fitting of each curve using a one-phase or two-phase association non-linear regression. All curves obtained in triplicates at room temperature.

The results displayed in **Figure 4.25** show that the addition of 50 μM BSH to the vesicles caused no alteration to the rate of proton flux upon addition of 50 mM KCl. At first, the addition of 50 μM E-BSH prior to 50 mM KCl seemed to enhance the rate of transport but the analysis of its negative control sample showed that this compound alone somehow causes proton leakage and dequenching of ACMA fluorescence, cancelling the former observation. Fitting of the curves and determination of the rate constants (**Table 4.3**) further supported this notion. Upon subtraction of the negative controls, no significant increase in the rate constant is visible.

Once again, both forms of bacillithiol failed to achieve what was expected: none showed any ability to interact with KhtTU.

4.6. Crystallography Studies on KhtT

At the moment, there is no structural information available for the proteins in the *khtSTU* operon. Since obtaining a three-dimensional structure of a protein is an important step in achieving a better understanding of its molecular properties, the crystallization of KhtT was attempted. At first, random screening for crystal-forming conditions using the vapor diffusion sitting-drop method was performed using apo-KhtT, concentrated up to 8-10 mg/mL, as described in section 3.11. This approach proved to be unsuccessful and screening was redone in the presence of 1 mM c-di-AMP. Two different crystallization conditions were identified with the Molecular Dimensions' commercial kit Wizard I&II: condition D10 (10% PEG8000; 100 mM Imidazole/HCl pH 8.0; 200 mM Calcium Acetate) and condition F11 (15% Reagent Alcohol[1]; 100 mM HEPES-NaOH pH 7.5; 200 mM $MgCl_2$), both using a protein concentration of 10 mg/mL and appearing only in plates incubated at 4ºC. Examples of these crystals are shown in **Figure 4.26**.

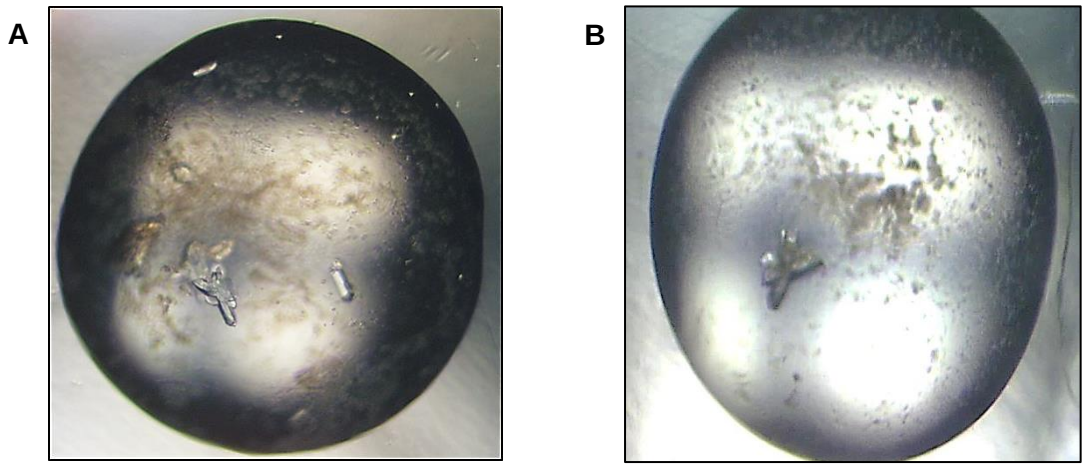

Figure 4.26 - Crystals obtained in the initial crystallization screening for KhtT incubated with c-di-AMP. The commercial kit used was Molecular Dimensions' Wizard I&II. **(A)** Condition D10: 10% PEG 8000; 100 mM Imidazole-HCl pH 8.0; 200 mM Calcium Acetate. **(B)** Condition F11: 15% Reagent Alcohol; 100 mM HEPES-NaOH pH 7.5; 200 mM $MgCl_2$. Both conditions were found using the following drop setup: 0.3 µL of reservoir solution + 0.3 µL of 10 mg/mL KhtT supplemented with 1 mM c-di-AMP, placed in a sitting-drop 96-well plate at 4ºC.

[1] Reagent Alcohol is composed of 90% ethanol, 5% isopropanol and 5% methanol.

Handmade screens around the two conditions were developed in order to reproduce crystals and optimize properties such as nucleation or size. These screens consisted on fine tuning around the initial condition using a range of the same (or similar) reagents as the commercial kit and bigger drop sizes (2 µL total volume, volume of initial screening drops was 0.6 µL). Both conditions (D10 and F11, shown in **Figure 4.26**) were successfully reproduced and optimized, with large, good-looking crystals appearing (examples shown in **Figure 4.27**).

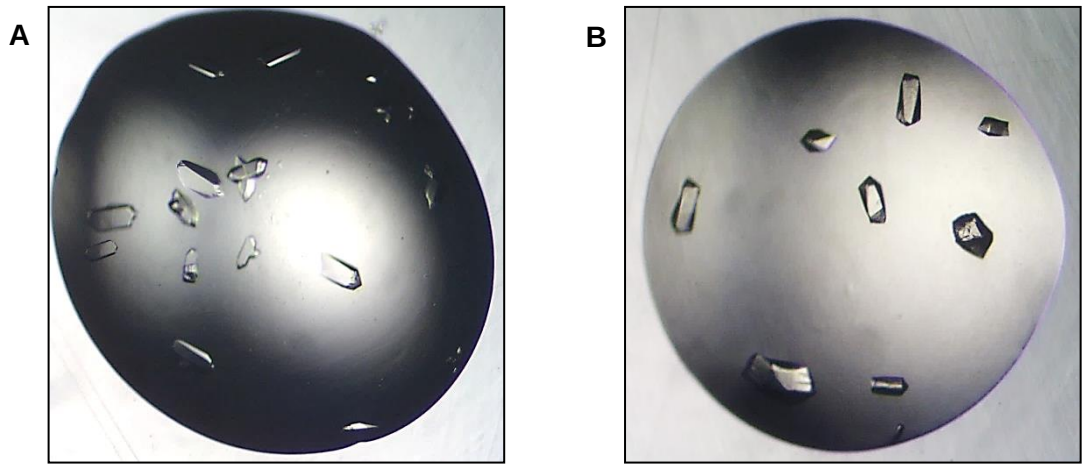

Figure 4.27 - Examples of KhtT + c-di-AMP crystals obtained with the handmade reproduction screens around conditions D10 and F11 from Molecular Dimensions' Wizard I&II screening kit. (A) Crystals obtained by screening around condition D10: crystals appeared in 10% PEG8000, 100 mM Imidazole-HCl pH 8.0 and calcium acetate ranging from 160 to 300 mM. **(B)** Crystals obtained by screening around condition F11: crystals appeared in 20% Reagent Alcohol, 100 mM HEPES-NaOH pH 7.5 and $MgCl_2$ ranging from 240 to 300 mM. Drops consisted on a mixture of 1 µL reservoir solution + 1 µL of 10 mg/mL KhtT previously incubated with 1 mM c-di-AMP in a 48-well plate set up at 4ºC.

The best-looking crystals were collected, soaked in cryoprotecting solutions (replicas of the reservoir solution of each well supplemented with 25% final concentration of glycerol or ethylene glycol), frozen in liquid nitrogen and analyzed by x-ray diffraction at the Soleil Synchrotron (Paris, France) at the Proxima I beamline. Crystals grown in conditions around D10 showed poor diffraction (7-8 Å of resolution) so no dataset was collected and this condition was abandoned. Crystals resulting from screens around condition F11 diffracted up to 2.3 Å, but the quality of the diffraction spots was not the best. Most of the reflections were streaky, making it harder to correctly index and integrate the spots (**Figure 4.28**). Still, several datasets were collected for further processing (statistical analysis of the top 2 datasets shown on **Table 4.4**). In order to solve the structure, three different strategies where applied: molecular replacement, crystallization of a selenomethionine-substituted KhtT and the incubation of native KhtT crystals with heavy atom solutions.

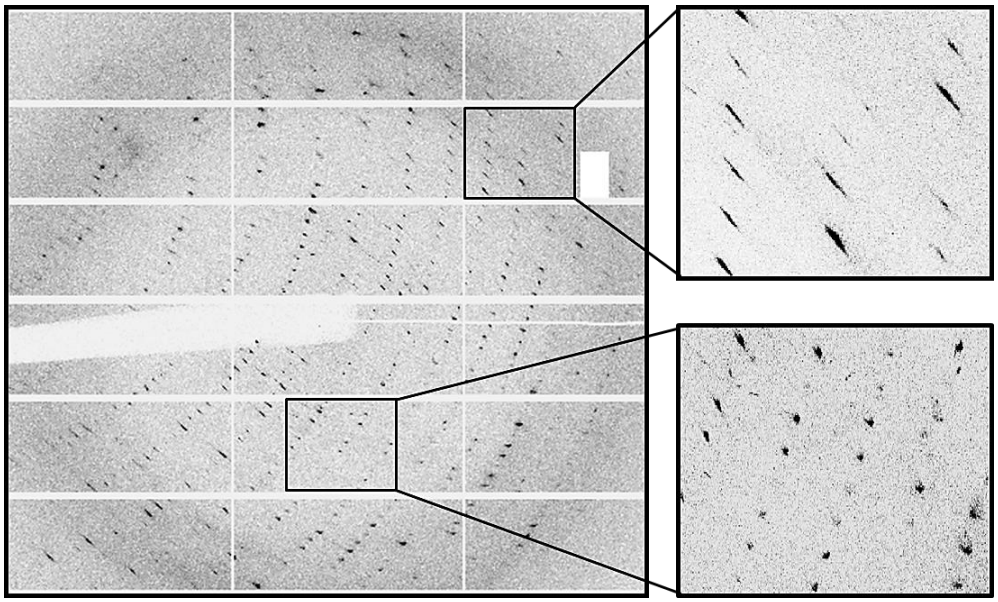

Figure 4.28 - Diffraction pattern of one of the KhtT + c-di-AMP crystals collected using synchrotron radiation at the Soleil Synchrotron in Paris, France. This crystal diffracted up to 2.3 Å, but most of the reflections were not properly indexed and integrated due to their streakiness. Comparison between bad spots (top) and good spots (bottom).

Table 4.4 - Summary of the statistical analysis of the top two datasets collected using KhtT+cdi-AMP crystals.

	Dataset 1			Dataset 2		
Resolution limit (Å)	2.29			2.84		
	Overall	Inner Shell	Outer Shell	Overall	Inner Shell	Outer Shell
Rmerge	0.204	0.145	0.853	0.197	0.098	0.737
Rmeas	0.213	0.152	0.891	0.207	0.103	0.775
Number of observations	221802			100866		
Number of unique observations	17418			9232		
I/(σI) at max res.	1.7			1.6		
cc1/2 at max res.	0.846			0.907		
Completeness at max res.	0.922			0.953		
Multiplicity at max res.	11.7			10.2		
Unit cell dimensions	a= 60.93; b=187.63; c= 66.65 (Å) α= 90; β= 90; γ= 90 (º)			a= 61.67; b= 185.46; c=66.33 (Å) α=90; β=90; γ=90 (º)		
Space Group:	C 2 2 2_1			C 2 2 2_1		

Molecular replacement was performed using models of C-terminal domains of RCK proteins either as single subunits or organized as dimers. The best solutions were obtained with the dimeric forms as indicated by higher Log of likelihood values, an indicator of the goodness of fit of a molecular model to the experimental data. However, the model corresponds to ~50% of the total protein mass in the crystal and the resulting electron-density maps were broken in the regions of the model and showed only small hints of regions corresponding to the N-terminal regions of the protein. Attempts to manually improve the model followed by refinement were not successful.

Crystals of selenomethionine-KhtT (SeMet-KhtT) incubated with c-di-AMP (examples shown in **Figure 4.29**) were obtained using the same handmade screens that yielded good-looking native KhtT crystals around the F11 condition. Simultaneously, heavy-atom derivatives of native KhtT crystals were prepared by overnight soaking of best looking crystals in a heavy-atom solution composed of a replica of the drop's well solution supplemented with 1 mM of a Heavy Atom (see Appendix, **Table 8.2**). Crystals were collected, soaked in cryoprotecting solution (replica of each well solution supplemented with 25% ethylene glycol) and analyzed at the Soleil X-ray synchrotron source.

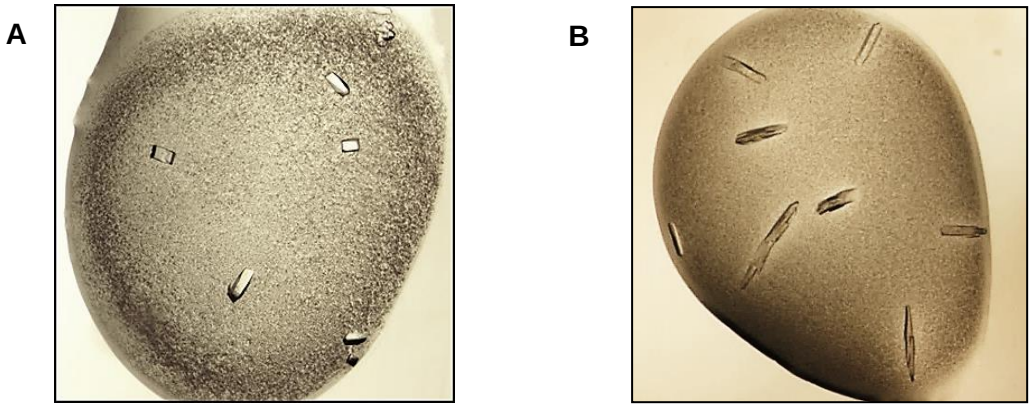

Figure 4.29 - Examples of SeMet-KhtT + c-di-AMP crystals obtained using handmade screens around condition F11 of Molecular Dimensions' Wizard I&II kit. (A) SeMet-KhtT + 1 mM c-di-AMP crystals obtained in 14% Reagent Alcohol, 12% PEG4000, 100 mM HEPES-NaOH pH 7.5 and 200 mM $MgCl_2$. **(B)** SeMet-KhtT + 1 mM c-di-AMP crystals obtained in 10% Isopropanol, 15% PEG4000, 100 mM HEPES-NaOH pH 7.5 and 200 mM $MgCl_2$. Drops consisted on a mixture of 1 µL reservoir solution + 1 µL of 10 mg/mL SeMet-KhtT previously incubated with 1 mM c-di-AMP in a 48-well plate set up at 4ºC.

Heavy-atom soaked crystals showed only very low resolution diffraction (worse than 6 Å). SeMet-KhtT crystals diffracted to better than 3 Å but suffered from the same problem detected in the native crystals: streaky spots reflected in very high R-factors at low resolution. Probably as consequence no anomalous signal was detected. Further efforts are needed to solve the structure of KhtT.

4.7. Cyclic di-AMP Binding Site Comparison

A crystallographic structure of the RCK_C domain the KtrA protein from *S. aureus* bound to c-di-AMP was published in 2015 [54], revealing a binding site formed in the interface of two monomers. The authors also performed an analysis of the binding site residues responsible for the affinity of the ligand and mapped the polar contacts between the protein and c-di-AMP (**Figure 4.30** A and C). Although it was not possible to obtain the structure of KhtT during the course of this work, it was possible to do a reasonable prediction of the residues composing the binding site of KhtT, by comparing the KtrA structure mentioned above with a 3D-model obtained using the protein structure homology modelling software Swiss-Model [63].

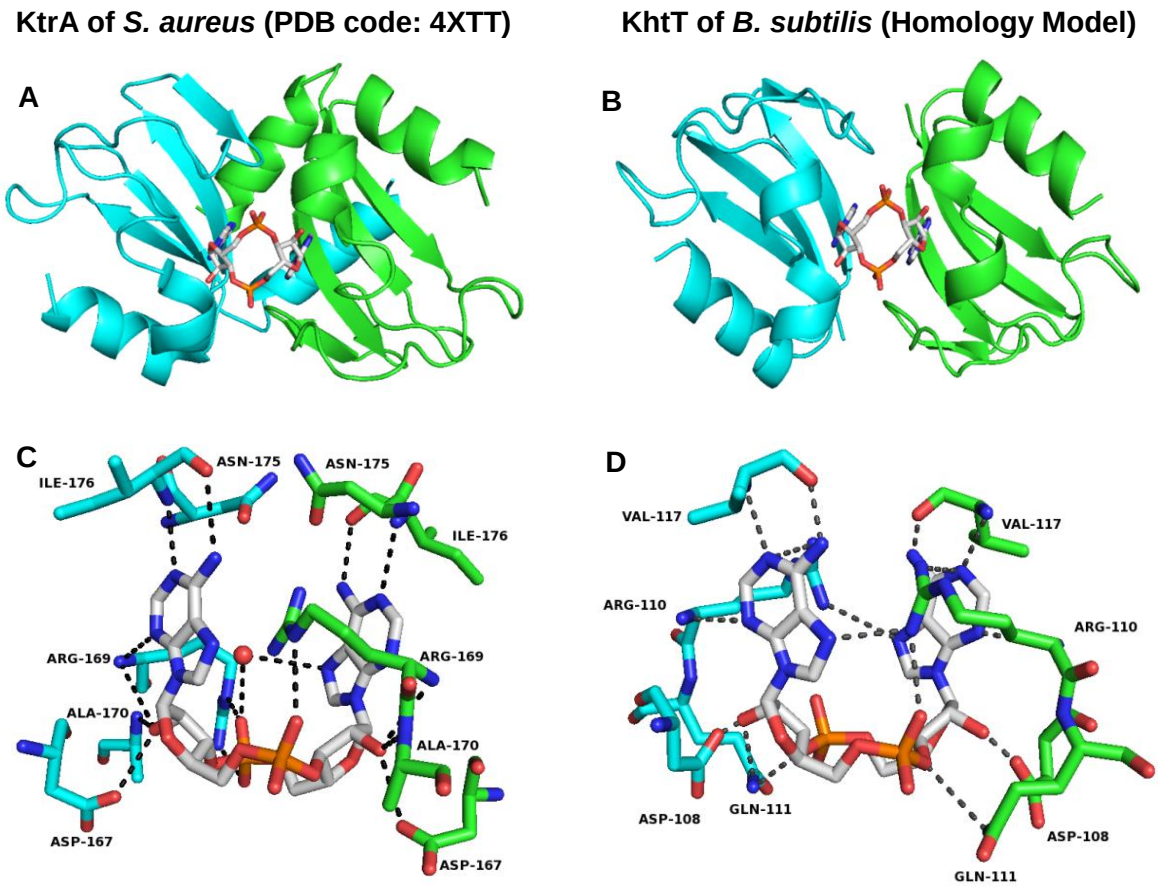

Figure 4.30 - Comparison of the c-di-AMP binding sites between the crystallographic structure of KtrA of *S. aureus* and a 3-D model of KhtT. (A) Structure of the KtrA RCK_C domain in complex with c-di-AMP (PDB code 4XTT); **(B)** Three dimensional model of a dimer of the RCK_C domain of KhtT, obtained by the structure modelling tool Swiss-Model. **(C)** The binding site residues that form direct hydrogen bonds with c-di-AMP in KtrA. **(D)** Residues that are predicted to form direct hydrogen bonds with c-di-AMP in KhtT. Cyclic di-AMP molecule is shown as white sticks. Protein monomers are shown in either cyan or green. The red sphere shown in **(C)** symbolizes a water molecule.

The structure of KtrA exhibits a binding site mainly composed of D167, R169, N175 along with A170 and I176. The pairwise sequence alignment of KtrA and KhtT (**Figure 4.31**) shows a relatively high sequence similarity in the binding site region (residues 110 to 125 of KhtT, highlighted by the red square). Thus, it is fairly safe to estimate that some of these conserved residues (such as the aspartate or the arginine) should be involved in the binding interactions between KhtT and c-di-AMP. According to the model prediction, we propose that the residues D108, R110, Q111 and V117 of both monomers form hydrogen bonds with c-di-AMP.

This prediction may be used to drive further experiments, such as site-direct mutagenesis studies, which would elucidate the impact of these residues in c-di-AMP binding to KhtT and to KhtTU.

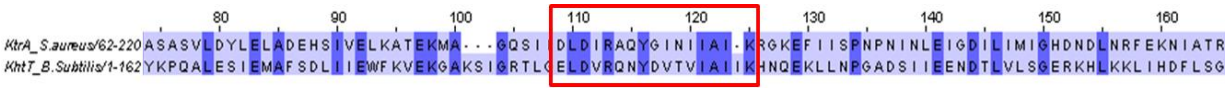

Figure 4.31 - Sequence alignment of the RCK_C segments of *S. aureus* KtrA and *B. subtilis* KhtT. The red square highlights the region of the residues that compose the binding site for c-di-AMP in KtrA and those predicted to do so in KhtT. Numbering above is relative to the residues of KhtT.

5. Conclusions

The main goals of this work were: First, the establishment of a working expression system for as many proteins of the *khtSTU* operon as possible, including the development of purification protocols for each of them; Second, the elucidation of the biochemical properties of KhtT as a regulator of the KhtU antiporter.

In summary, this work established large-scale expression and purification protocols for KhtT and KhtU (as a KhtTU complex) but not for KhtS. Ligand screening for KhtT was concluded with one hit, c-di-AMP. This ligand binds to KhtT with high affinity and specificity (c-di-GMP does not bind) and a stoichiometry of 1:2, stabilizing its structure. Upon establishing a functional assay for KhtTU, the impact of c-di-AMP on its activity was studied. C-di-AMP enhances antiport activity of KhtTU almost 10-fold. The literature-based hypothesis of bacillithiol being a ligand of KhtTU was also explored, but no evidence supporting this conjecture was obtained. Crystallization trials for KhtT in the presence of c-di-AMP were carried out and at least one workable condition was found. Several datasets with resolution as high as 2.3 Å were collected. However, insufficient quality of the data along with difficulty in solving the phase problem rendered the determination of the protein structure unfeasible at this stage.

The role of *khtS* in the *khtSTU* operon could not be clarified in this work. No significant protein expression was achieved in any of the conditions tested. There are several possible explanations for this. One is that the protein is too unstable to be expressed alone. Another is this genomic region was misannotated and it is not an ORF but a regulatory element of the *khtSTU* operon. For example, KtrAB and KimA are preceded by a riboswitch, which controls the transcription of these proteins.

The identification of c-di-AMP as a ligand of KhtTU adds another layer of understanding of the *Bacillus subtilis'* potassium homeostasis machinery. This data strongly indicates that the same ligand regulates the activity of multiple proteins involved in potassium homeostasis: KimA, KtrAB and now KhtTU. Its effect as an activator of KhtTU fits with the expected role of this protein complex in lowering internal concentrations of potassium in the late stages of hyperosmotic adaptation and also with reports of increased c-di-AMP concentration when intracellular potassium is high. We can speculate that high intracellular potassium will lead to an increase in c-di-AMP which by activating KhtTU will lead to the rapid export of potassium, restoring homeostatic levels. While there is no evidence of c-di-AMP changes due to alterations

in intracellular pH, if KhtTU has a role in alkali resistance by importing H^+ it is possible that c-di-AMP is also involved in the regulation of this process.

ITC established a K_D of 138 nM while the functional assay led to the determination of an EC_{50} of 1.97 µM. ITC was performed with KhtT alone, so what was measured was the strength of the interaction between the ligand and this protein. In the antiporter assay what was measured was the effect of the ligand on the whole KhtTU complex. It makes sense that the EC_{50} is higher than the K_D since that in the case of the complex the binding energy of the ligand is going to be used to induce a conformation change not just in KhtT but also on the membrane protein. In fact, the K_D measured by ITC is much lower than the intracellular concentration of c-di-AMP between 2 and 5 µM reported for *B. subtilis* [49], which would make regulation of KhtT impossible. In contrast, the EC_{50} of ~2 µM falls within the physiological range, further supporting a regulatory role of c-di-AMP for KhtTU.

6. Future Perspectives

Future work for this project includes but is not limited to the following topics:

First, it would be interesting to further characterize the binding of c-di-AMP to KhtT, possibly with site-directed mutagenesis studies of the residues that were predicted to be part of the binding site. Also, the development of a functional assay for KhtTU using liposomes reconstituted with this complex would also expand our toolkit and allow a different approach for the characterization of this system. Coupling this assay with the visualization of antiport using radioactive ^{86}Rb would give us a direct measurement of cation transport by KhtTU and a more controlled environment.

The execution of the vesicle antiporter assay after cloning the whole *khtSTU* operon would also be an interesting follow-up experiment. Now that the activity of KhtTU was determined using this assay, any differences arising from the inclusion of the *khtS* gene would provide information about the importance of this gene.

It is also vital to resume the crystallographic studies of KhtT by finding new and better crystallization conditions, which together with the use of the selenomethionine variant and/or heavy atom derivatization would hopefully allow the resolution of the phase problem for the datasets obtained, rendering the structure for KhtT in complex with c-di-AMP. Still regarding crystallography, another perspective is the start of crystallization studies of the KhtTU complex, the structure of which would provide valuable information about the molecular properties of this system.

7. References

1. Lodish H, Berk A, Zipursky SL et al. - *Molecular Cell Biology 4th edition* - Section 15.4: Intracellular Ion Environment and Membrane Electric Potential. New York. W. H. Freeman (2000).

2. Epstein, W. - The Roles and Regulation of Potassium in Bacteria. *Prog. Nucleic Acid Res. Mol. Biol.* **75,** 293–320 (2003).

3. Epstein, W. - Osmoregulation by potassium transport in *Escherichia coli*. *FEMS Microbiol. Rev.* **2,** 73–78 (1986).

4. Gundlach, J. *et al.* - Adaptation of Bacillus subtilis to Life at Extreme Potassium Limitation. *mBio.* **8,** 1–12 (2017).

5. McLaggan, D., Naprstek, J., Buurman, E. T. & Epstein, W. - Interdependence of K^+ and glutamate accumulation during osmotic adaptation of *Escherichia coli*. *J. Biol. Chem.* **269,** 1911–1917 (1994).

6. Whatmore, M., Chudek, J. & Reed, R.H. - The effects of osmotic upshock on the intracellular solute pools of *Bacillus subtilis*. *J. Gen. Microbiol.* **136,** 2527–2535 (1990).

7. Meury, J., Robin, A. & Monnier-Champeix, P. - Turgor-controlled K^+ fluxes and their pathways in *Escherichia coli*. *Eur. J. Biochem.* **151,** 613–619 (1985).

8. Holtmann, G., Bakker, E. P., Uozumi, N. & Bremer, E. - KtrAB and KtrCD: two K^+ uptake systems in *Bacillus subtilis* and their role in adaptation to hypertonicity. *J Bacteriol* **185,** 1289–1298 (2003).

9. Hoffmann, T. & Bremer, E. - Management of Osmotic Stress by *Bacillus Subtilis* : Genetics and Physiology. *Stress Environ. Regul. Gene Expr. Adapt. Bact.* 657–676 (2016).

10. Kroll, R. G. & Booth, I. R. - The relationship between intracellular pH, the pH gradient and potassium transport in *Escherichia coli*. *Biochem. J.* **216,** 709–16 (1983).

11. Kroll, R. G. & Booth, I. R. - The role of potassium transport in the generation of a pH gradient in *Escherichia coli*. *Biochem. J.* **198,** 691–8 (1981).

12. Prince, W. S. & Villarejo, M. R. - Osmotic control of proU transcription is mediated through direct action of potassium glutamate on the transcription complex. *J. Biol. Chem.* **265,** 17673–17679 (1990).

13. Lundberg, M. E., Becker, E. C. & Choe, S. - MstX and a Putative Potassium Channel Facilitate Biofilm Formation in *Bacillus subtilis*. *PLoS One* **8**(5)**,** (2013).

14. Suelter, C. H. - Enzymes activated by monovalent cations. *Science.* **168,** 789–95 (1970).

15. Nissen, P., Hansen, J., Ban, N., Moore, P. B. & Steitz, T. A. - The structural basis of ribosome activity in peptide bond synthesis. *Science* **289,** 920–30 (2000).

16. Gralla, J. D. & Vargas, D. R. - Potassium glutamate as a transcriptional inhibitor during bacterial osmoregulation. *EMBO J.* **25,** 1515–1521 (2006).

17. Hodgkin, A. L. - The electrical basis of electrical activity in nerve and muscle. *Biological Reviews* **26,** 339–409 (1951).

18. Baylor, D. A. & Nicholls, J. G. - Changes In Extracellular Potassium Concentration Produced By Neuronal Activity In The Central Nervous System Of The Leech. *J. Physiol.* **203**, 555–569 (1969).

19. Karaki, H., Urakawa, N. & Kutsky, P. - Potassium-induced contraction in smooth muscle. *Nihon Heikatsukin Gakkai Zasshi* **20,** 427–444 (1984).

20. Nakamura, Y., Ohya, Y., Abe, I. & Fujishima, M. - Sodium-potassium pump current in smooth muscle cells from mesenteric resistance arteries of the guinea-pig. *J. Physiol.* **519,** 203–212 (1999).

21. Bueno-orovio, A. - Na/K pump regulation of cardiac repolarization: insights from a systems biology approach - Springer. *Eur. J. Physiol.* **466,** 183–193 (2014).

22. Nørgaard, A. *et al.* - The concentration of the Na/K pump in skeletal and heart muscle in congestive heart failure. *Int. J. Cardiol.* **26,** 185–190 (1990).

23. Giraldez, T. & Rothberg, B. S. - Understanding the conformational motions of RCK gating rings. *J. of General Physiology* **149**(4), 431-441 (2017).

24. Diskowski, M. *et al.* - Helical jackknives control the gates of the double-pore K^+ uptake system KtrAB. *Elife* **6,** 1–21 (2017).

25. Albright, R. A., Ibar, J. L. V., Kim, C. U., Gruner, S. M. & Morais-Cabral, J. H. - The RCK Domain of the KtrAB K+ Transporter: Multiple Conformations of an Octameric Ring. *Cell* **126,** 1147–1159 (2006).

26. Vieira-Pires, R. S., Szollosi, A. & Morais-Cabral, J. H. - The structure of the KtrAB potassium transporter. *Nature* **496,** 323–8 (2013).

27. Roosild, T. P., Miller, S., Booth, I. R. & Choe, S. - A mechanism of regulating transmembrane potassium flux through a ligand-mediated conformational switch. *Cell* **109,** 781–791 (2002).

28. Smith, F. J., Pau, V. P. T., Cingolani, G. & Rothberg, B. S. - Structural basis of allosteric interactions among Ca2þ-binding sites in a Kþ channel RCK domain. *Nat. Commun.* **4,** 1–10 (2013).

29. Gundlach, J. *et al.* - Control of potassium homeostasis is an essential function of the second messenger cyclic di-AMP in *Bacillus subtilis*. *Sci. Signal.* **10,** eaal3011 (2017).

30. Szollosi, A., Vieira-Pires, R. S., Teixeira-Duarte, C. M., Rocha, R. & Morais-Cabral, J. H. - Dissecting the Molecular Mechanism of Nucleotide-Dependent Activation of the KtrAB K^+ Transporter. *PLoS Biol.* **14**(1) (2016).

31. Ferguson, G. P., Nikolaev, Y., McLaggan, D., Maclean, M. & Booth, I. R. - Survival during exposure to the electrophilic reagent N-ethylmaleimide in *Escherichia coli*: Role of KefB and KefC potassium channels. *J. Bacteriol.* **179,** 1007–1012 (1997).

32. Ness, L. S. & Booth, I. R. - Different foci for the regulation of the activity of the KefB and KefC glutathione-gated K^+ efflux systems. *J. Biol. Chem.* **274,** 9524–9530 (1999).

33. Healy, J. *et al.* - Understanding the Structural Requirements for Activators of the Kef Bacterial Potassium Efflux System. *Biochemistry.* **53**(12):1982-92 (2014).

34. Prindle, A. *et al.* - Ion channels enable electrical communication in bacterial communities. *Nature* **527,** 59–63 (2015).

35. Fujisawa, M., Ito, M. & Krulwich, T. A. - Three two-component transporters with channel-like properties have monovalent cation/proton antiport activity. *Proc. Natl. Acad. Sci. U. S. A.* **104,** 13289–13294 (2007).

36. Fujisawa, M., Wada, Y. & Ito, M. Modulation of the K^+ efflux activity of *Bacillus subtilis* YhaU by YhaT and the C-terminal region of YhaS. *FEMS Microbiol. Lett.* **231,** 211–217 (2004).

37. Moszer, I., Jones, L. M., Moreira, S., Fabry, C. & Danchin, A. - SubtiList: the reference database for the *Bacillus subtilis* genome. *Nucleic Acids Res.* **30,** 62–65 (2002).

38. Michna, R. H., Zhu, B., Mäder, U. & Stülke, J. - SubtiWiki 2.0--an integrated database for the model organism *Bacillus subtilis*. *Nucleic Acids Res.* **44,** D654-62 (2016).

39. Helmann, J. D. *et al.* - Global Transcriptional Response of *Bacillus subtilis* to Heat Shock. *J Bacteriol* **183,** 7318 (2001).

40. Wiegert, T., Homuth, G., Versteeg, S. & Schumann, W. - Alkaline shock induces the *Bacillus subtilis* sigma(W) regulon. *Mol. Microbiol.* **41,** 59–71 (2001).

41. Cao, M. *et al.* - Defining the *Bacillus subtilis* sigma(W) regulon: a comparative analysis of promoter consensus search, run-off transcription/macroarray analysis (ROMA), and transcriptional profiling approaches. *J. Mol. Biol.* **316,** 443–457 (2002).

42. Chandrangsu, P., Dusi, R., Hamilton, C. J. & Helmann, J. D. - Methylglyoxal resistance in *Bacillus subtilis* : contributions of bacillithiol-dependent and independent pathways. *Mol. Microbiol.* **91,** 706–715 (2014).

43. Ferguson, G. P., Munro, A. W., Douglas, R. M., McLaggan, D. & Booth, I. R. - Activation of potassium channels during metabolite detoxification in *Escherichia coli*. *Mol. Microbiol.* **9,** 1297–1303 (1993).

44. Ferguson, G. P., Mclaggan, D. & Booth, L. R. - Potassium channel activation by glutathione-S-conjugates in *Escherichia coil*: protection against methylglyoxal is mediated by cytoplasmic acidification. *Mol. Microbiol.* **17,** 1025–1033 (1995).

45. Roosild, T. P., Castronovo, S., Healy, J., Miller, S. & Pliotas, C. - Mechanism of ligand-gated potassium efflux in bacterial pathogens. *PNAS* **107**(46):19784-9 (2010).

46. Ozyamak, E. *et al.* - The critical role of S-lactoylglutathione formation during methylglyoxal detoxification in *Escherichia coli*. *Mol. Microbiol.* **78,** 1577–1590 (2010).

47. Corrigan, R. M. & Gründling, A. - Cyclic di-AMP: another second messenger enters the fray. *Nat. Rev. Microbiol.* **11,** 513–524 (2013).

48. Commichau, F. M., Dickmanns, A., Gundlach, J., Ficner, R. & Stülke, J. - A jack of all trades: The multiple roles of the unique essential second messenger cyclic di-AMP. *Mol. Microbiol.* **97,** 189–204 (2015).

49. Oppenheimer-Shaanan, Y., Wexselblatt, E., Katzhendler, J., Yavin, E. & Ben-Yehuda, S. - c-di-AMP reports DNA integrity during sporulation in *Bacillus subtilis*. *EMBO Rep.* **12,** 594–601 (2011).

50. Kalia, D. *et al.* - Nucleotide, c-di-GMP, c-di-AMP, cGMP, cAMP, (p)ppGpp signaling in bacteria and implications in pathogenesis. *Chem. Soc. Rev.* **42,** 305–341 (2013).

51. Fahmi, T., Port, G. & Cho, K. - c-di-AMP: An Essential Molecule in the Signaling Pathways that Regulate the Viability and Virulence of Gram-Positive Bacteria. *Genes (Basel).* **8**(8) E197 (2017).

52. Gundlach, J. *et al.* - Control of potassium homeostasis is an essential function of the second messenger cyclic di-AMP in *Bacillus subtilis*. *Sci. Signal.* **10,** eaal3011 (2017).

53. Corrigan, R. M. *et al.* - Systematic identification of conserved bacterial c-di-AMP receptor proteins. *PNAS* **110**(22) 9084-9089 (2013).

54. Kim, H. *et al.* - Structural studies of potassium transport protein KtrA regulator of conductance of K^+ (RCK) C domain in complex with cyclic diadenosine monophosphate (c-di-AMP). *J. Biol. Chem.* **290,** 16393–16402 (2015).

55. Humphries, E. S. a. & Dart, C. - Neuronal and Cardiovascular Potassium Channels as Therapeutic Drug Targets: Promise and Pitfalls. *J. Biomol. Screen.* **20,** 1055–1073 (2015).

56. Sanguinetti, M. C. & Spector, P. S. - Potassium channelopathies. *Neuropharmacology* **36,** 755–762 (1997).

57. Ashcroft, F. M. - ATP-sensitive potassium channelopathies: Focus on insulin secretion. *J. Clin. Invest.* **115,** 2047–2058 (2005).

58. Stühmer, W., Alves, F., Hartung, F., Zientkowska, M. & Pardo, L. A. - Potassium channels as tumour markers. *FEBS Lett.* **580,** 2850–2852 (2006).

59. Stanton, T. B. - A call for antibiotic alternatives research. *Trends Microbiol.* **21,** 111–113 (2013).

60. Gries, C. M., Bose, J. L., Nuxoll, A. S., Fey, P. D. & Bayles, K. W. - The Ktr potassium transport system in *Staphylococcus aureus* and its role in cell physiology, antimicrobial resistance and pathogenesis. *Mol. Microbiol.* **89,** 760–773 (2013).

61. Su, J., Gong, H., Lai, J., Main, A. & Lu, S. - The potassium transporter trk and external potassium modulate *Salmonella enterica* protein secretion and virulence. *Infect. Immun.* **77,** 667–675 (2009).

62. Castañeda-García, A., Do, T. T. & Blázquez, J. - The K^+ uptake regulator trka controls membrane potential, pH homeostasis and multidrug susceptibility in *Mycobacterium smegmatis*. *J. Antimicrob. Chemother.* **66,** 1489–1498 (2011).

63. Biasini, M. *et al.* - SWISS-MODEL: Modelling protein tertiary and quaternary structure using evolutionary information. *Nucleic Acids Res.* **42,** 252–258 (2014).

64. Niesen, F. H., Berglund, H. & Vedadi, M. - The use of differential scanning fluorimetry to detect ligand interactions that promote protein stability. *Nat. Protoc.* **2,** 2212–2221 (2007).

65. Freyer, M. W. & Lewis, E. A. - Isothermal Titration Calorimetry: Experimental Design, Data Analysis, and Probing Macromolecule/Ligand Binding and Kinetic Interactions. *Methods Cell Biol.* **84,** 79–113 (2008).

66. Rosen, B. P - Ion Extrusion Systems in *Escherichia Coli*. *Methods in Enzymology.* **125** 328-336 (1986).

.

8. Appendix

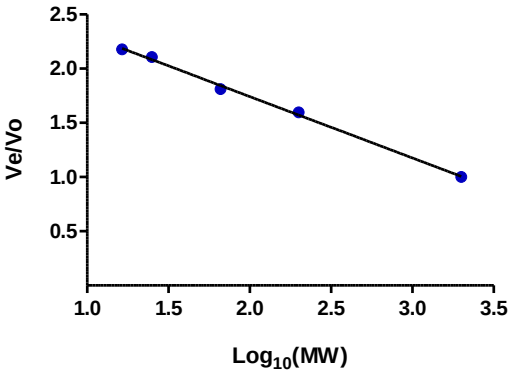

$$\frac{Ve}{Vo} = -0.566 Log_{10}(MW) + 2.875 \ \ (R^2 = 0.997)$$

Table 8.1 – Standards used for the calibration of the Superdex 200 10/300 GL gel filtration column (GE Healthcare) used in this work.

Standard Used	Molecular Weight (kDa)	Elution Volume (mL)
Blue Dextran	2000	8.45
β-amylase	200	13.5
Albumin	66	15.3
Chymotrypsinogen A	25	17.8
Ribonuclease A	16.4	18.4

Figure 8.1 - Calibration curve for Superdex 200 10/300 GL gel filtration column (GE Healthcare). Obtained using pure samples of the standards shown in Table 8.1. Each standard was loaded separately and sequentially. Buffer used was the same as KhtT buffer (20 mM Tris pH 8.0; 150 mM KCl) supplemented with 2 mM DTT. Calibration equation below the graph.

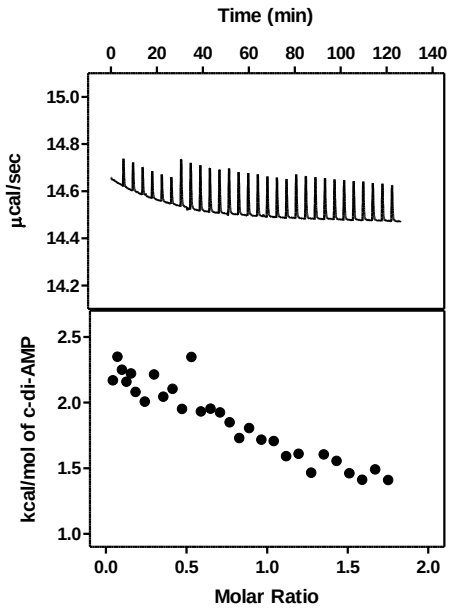

Figure 8.2 - Representative curve of KhtT ITC Buffer being titrated with 300 µM c-di-AMP. The top panel shows the thermogram obtained. The bottom panel shows the binding isotherm after normalization and integration of the raw data. Performed at 25ºC.

Table 8.2 - Heavy atom stock solutions used in heavy atom derivatization of native KhtT+cdiAMP crystals.

Heavy Atom Solution	Heavy atom	Stock concentration
4-(Hydroxymercurio)benzoic acid	Hg	5 mM
Ethylmercury chloride	Hg	5 mM
Mercury(II) potassium iodide	Hg	5 mM
Tetrakis(acetoxymercuri)methane	Hg	5 mM
Methylmercury(II) chloride	Hg	10 mM
Gold(I) potassium cyanide	Au	5 mM
Potassium platinum(II) chloride	Pt	1 mM
Dichloro(ethylenediamine)platinum(II)	Pt	5 mM
Di-μ-chloro-dichlorobis(ethylene)diplatinum (II)	Pt	10 mM

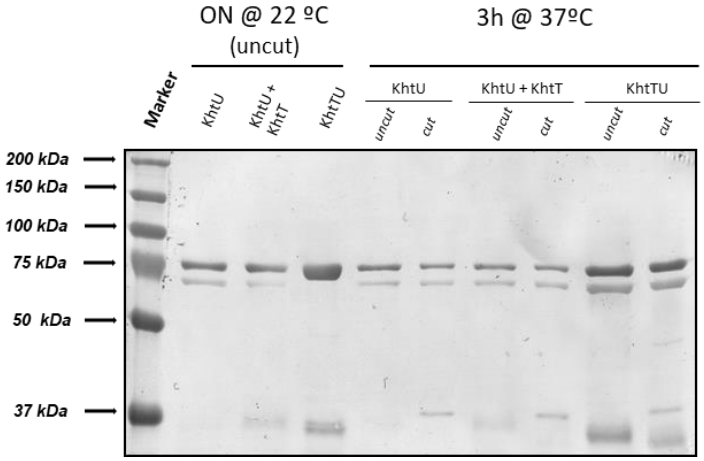

Figure 8.3 - Ponceau staining of the Western Blot membrane shown in Figure 4.8. The membrane used for the Western Blotting visualization of KhtU Expression Test samples was stained with Ponceau S for detection of total protein in the membrane, as a positive control.

KhtT Crystallography Handmade Screens Composition

Composition of the 48 well handmade screens around condition D10 from Wizard I&II commercial kit (10% PEG8000; 100 mM Imidazole/HCl pH 8.0; 200 mM Calcium Acetate) used in crystallization studies of KhtT supplemented with 1 mM c-di-AMP. Description of the components of each coordinate at the top right corner of each table.

Buffer used in all D10 screens: 100 mM Imidazole/HCl pH 8.0

Table 8.3 – Composition of handmade screens around condition D10 (D10.1 to D10.3).

D10.1	**1**	**2**	**3**	**4**	**5**	**6**	
A	*7.5*	*10.0*	*12.5*	*15.0*	*20.0*	*25.0*	**% PEG8000**
	160	*160*	*160*	*160*	*160*	*160*	**mM CaAcetate**
B	*7.5*	*10.0*	*12.5*	*15.0*	*20.0*	*25.0*	
	180	*180*	*180*	*180*	*180*	*180*	
C	*7.5*	*10.0*	*12.5*	*15.0*	*20.0*	*25.0*	
	200	*200*	*200*	*200*	*200*	*200*	
D	*7.5*	*10.0*	*12.5*	*15.0*	*20.0*	*25.0*	
	220	*220*	*220*	*220*	*220*	*220*	
E	*7.5*	*10.0*	*12.5*	*15.0*	*20.0*	*25.0*	
	240	*240*	*240*	*240*	*240*	*240*	
F	*7.5*	*10.0*	*12.5*	*15.0*	*20.0*	*25.0*	
	260	*260*	*260*	*260*	*260*	*260*	
G	*7.5*	*10.0*	*12.5*	*15.0*	*20.0*	*25.0*	
	280	*280*	*280*	*280*	*280*	*280*	
H	*7.5*	*10.0*	*12.5*	*15.0*	*20.0*	*25.0*	
	300	*300*	*300*	*300*	*300*	*300*	

D10.2	1	2	3	4	5	6	
A	12.0	12.5	13.0	12.0	12.5	13.0	% PEG8000
	200	200	200	200	200	200	mM CaAcetate
B	12.0	12.5	13.0	12.0	12.5	13.0	
	210	210	210	210	210	210	
C	12.0	12.5	13.0	12.0	12.5	13.0	
	220	220	220	220	220	220	
D	12.0	12.5	13.0	12.0	12.5	13.0	
	240	240	240	240	240	240	
E	12.0	12.5	13.0	12.0	12.5	13.0	
	240	240	240	240	240	240	
F	12.0	12.5	13.0	12.0	12.5	13.0	
	260	260	260	260	260	260	
G	12.0	12.5	13.0	12.0	12.5	13.0	
	280	280	280	280	280	280	
H	12.0	12.5	13.0	12.0	12.5	13.0	
	300	300	300	300	300	300	

D10.3	1	2	3	4	5	6	
A	8.0	9.0	10.0	11.0	12.0	13.0	% PEG8000
	200	200	200	200	200	200	mM CaAcetate
B	8.0	9.0	10.0	11.0	12.0	13.0	
	210	210	210	210	210	210	
C	8.0	9.0	10.0	11.0	12.0	13.0	
	220	220	220	220	220	220	
D	8.0	9.0	10.0	11.0	12.0	13.0	
	240	240	240	240	240	240	
E	8.0	9.0	10.0	11.0	12.0	13.0	
	240	240	240	240	240	240	
F	8.0	9.0	10.0	11.0	12.0	13.0	
	260	260	260	260	260	260	
G	8.0	9.0	10.0	11.0	12.0	13.0	
	280	280	280	280	280	280	
H	8.0	9.0	10.0	11.0	12.0	13.0	
	300	300	300	300	300	300	

Composition of the 48 well handmade screens around condition F11 from Wizard I&II commercial kit (15% Reagent Alcohol[2]; 100 mM HEPES-NaOH pH 7.5; 200 mM $MgCl_2$) used in crystallization studies of KhtT supplemented with 1 mM c-di-AMP. Description of the components of each coordinate at the top right corner of each table.

Buffer used in all F11 screens: 100 mM HEPES-NaOH pH 7.5

Table 8.4 - Composition of handmade screens around condition F11 (F11.1 to F11.9).

F11.1	**1**	**2**	**3**	**4**	**5**	**6**	
A	*10*	*15*	*20*	*25*	*30*	*40*	**% Reagent Alcohol**
	160	*160*	*160*	*160*	*160*	*160*	**mM MgCl2**
B	*10*	*15*	*20*	*25*	*30*	*40*	
	180	*180*	*180*	*180*	*180*	*180*	
C	*10*	*15*	*20*	*25*	*30*	*40*	
	200	*200*	*200*	*200*	*200*	*200*	
D	*10*	*15*	*20*	*25*	*30*	*40*	
	220	*220*	*220*	*220*	*220*	*220*	
E	*10*	*15*	*20*	*25*	*30*	*40*	
	240	*240*	*240*	*240*	*240*	*240*	
F	*10*	*15*	*20*	*25*	*30*	*40*	
	260	*260*	*260*	*260*	*260*	*260*	
G	*10*	*15*	*20*	*25*	*30*	*40*	
	280	*280*	*280*	*280*	*280*	*280*	
H	*10*	*15*	*20*	*25*	*30*	*40*	
	300	*300*	*300*	*300*	*300*	*300*	

[2] Reagent Alcohol is composed of 90% Ethanol, 5% Isopropanol and 5% Methanol.

F11.2	1	2	3	4	5	6
A	18	19	20	21	22	23
	180	180	180	180	180	180
B	18	19	20	21	22	23
	190	190	190	190	190	190
C	18	19	20	21	22	23
	200	200	200	200	200	200
D	18	19	20	21	22	23
	210	210	210	210	210	210
E	18	19	20	21	22	23
	220	220	220	220	220	220
F	18	19	20	21	22	23
	230	230	230	230	230	230
G	18	19	20	21	22	23
	240	240	240	240	240	240
H	18	19	20	21	22	23
	250	250	250	250	250	250

% Reagent Alcohol
mM MgCl2

	+ PEG400			+ PEG 4000			+ Ethylene Glycol		
F11.3	1	2	3	4	5	6	7	8	9
A	10	12	15	10	12	15	10	12	15
	5	5	5	5	5	5	5	5	5
B	10	12	15	10	12	15	10	12	15
	7.5	7.5	7.5	7.5	7.5	7.5	7.5	7.5	7.5
C	10	12	15	10	12	15	10	12	15
	10	10	10	10	10	10	10	10	10
D	10	12	15	10	12	15	10	12	15
	12.5	12.5	12.5	12.5	12.5	12.5	12.5	12.5	12.5
E	10	12	15	10	12	15	10	12	15
	15	15	15	15	15	15	15	15	15
F	10	12	15	10	12	15	10	12	15
	20	20	20	20	20	20	20	20	20
G	10	12	15	10	12	15	10	12	15
	22.5	22.5	22.5	22.5	22.5	22.5	22.5	22.5	22.5
H	10	12	15	10	12	15	10	12	15
	25	25	25	25	25	25	25	25	25

($MgCl_2$ was fixed at 200 mM)

% Reagent Alcohol
% PEG/Ethylene Glycol

F11.4	1	2	3	4	5	6
A	5	10	15	20	25	30
	5	5	5	5	5	5
B	5	10	15	20	25	30
	7.5	7.5	7.5	7.5	7.5	7.5
C	5	10	15	20	25	30
	10	10	10	10	10	10
D	5	10	15	20	25	30
	12.5	12.5	12.5	12.5	12.5	12.5
E	5	10	15	20	25	30
	15	15	15	15	15	15
F	5	10	15	20	25	30
	20	20	20	20	20	20
G	5	10	15	20	25	30
	22.5	22.5	22.5	22.5	22.5	22.5
H	5	10	15	20	25	30
	25	25	25	25	25	25

($MgCl_2$ was fixed at 200 mM)
% Isopropanol
% PEG4000

F11.5	1	2	3	4	5	6
A	5	10	15	20	25	30
	5	5	5	5	5	5
B	5	10	15	20	25	30
	7.5	7.5	7.5	7.5	7.5	7.5
C	5	10	15	20	25	30
	10	10	10	10	10	10
D	5	10	15	20	25	30
	12.5	12.5	12.5	12.5	12.5	12.5
E	5	10	15	20	25	30
	15	15	15	15	15	15
F	5	10	15	20	25	30
	20	20	20	20	20	20
G	5	10	15	20	25	30
	22.5	22.5	22.5	22.5	22.5	22.5
H	5	10	15	20	25	30
	25	25	25	25	25	25

($MgCl_2$ was fixed at 200 mM)
%1,2-Propanediol
% PEG4000

F11.6	1	2	3	4	5	6
A	5	10	15	20	25	30
	5	5	5	5	5	5
B	5	10	15	20	25	30
	7.5	7.5	7.5	7.5	7.5	7.5
C	5	10	15	20	25	30
	10	10	10	10	10	10
D	5	10	15	20	25	30
	12.5	12.5	12.5	12.5	12.5	12.5
E	5	10	15	20	25	30
	15	15	15	15	15	15
F	5	10	15	20	25	30
	20	20	20	20	20	20
G	5	10	15	20	25	30
	22.5	22.5	22.5	22.5	22.5	22.5
H	5	10	15	20	25	30
	25	25	25	25	25	25

($MgCl_2$ was fixed at 200 mM)

%1,4-Butanediol

% PEG4000

F11.7	1	2	3	4	5	6
A	10	15	20	25	30	35
	160	160	160	160	160	160
B	10	15	20	25	30	35
	180	180	180	180	180	180
C	10	15	20	25	30	35
	200	200	200	200	200	200
D	10	15	20	25	30	35
	220	220	220	220	220	220
E	10	15	20	25	30	35
	240	240	240	240	240	240
F	10	15	20	25	30	35
	260	260	260	260	260	260
G	10	15	20	25	30	35
	280	280	280	280	280	280
H	10	15	20	25	30	35
	300	300	300	300	300	300

% Isopropanol

mM MgCl2

F11.8	1	2	3	4	5	6	
A	15	20	25	30	35	40	% 1,4-Butanediol
	160	160	160	160	160	160	mM MgCl2
B	15	20	25	30	35	40	
	180	180	180	180	180	180	
C	15	20	25	30	35	40	
	200	200	200	200	200	200	
D	15	20	25	30	35	40	
	220	220	220	220	220	220	
E	15	20	25	30	35	40	
	240	240	240	240	240	240	
F	15	20	25	30	35	40	
	260	260	260	260	260	260	
G	15	20	25	30	35	40	
	280	280	280	280	280	280	
H	15	20	25	30	35	40	
	300	300	300	300	300	300	

F11.9	1	2	3	4	5	6	
A	10	12	14	16	18	20	% Reagent Alcohol
	10	10	10	10	10	10	% PEG4000
B	10	12	14	16	18	20	
	12	12	12	12	12	12	
C	10	12	14	16	18	20	
	14	14	14	14	14	14	
D	10	12	14	16	18	20	
	16	16	16	16	16	16	
E	10	12	14	16	18	20	
	18	18	18	18	18	18	
F	10	12	14	16	18	20	
	20	20	20	20	20	20	
G	10	12	14	16	18	20	
	22	22	22	22	22	22	
H	10	12	14	16	18	20	
	24	24	24	24	24	24	